BMPs from binding their cognate receptors [7–9]. One class of BMP antagonists possesses a secretory signal peptide and cysteine-rich domain, forming a subfamily of the cystine-knot superfamily of secreted factors [7].

BMP-7, the most abundant BMP in the fetal and adult kidney, is required for normal kidney development in mammals; *BMP7* null mice die shortly postpartum due to renal dysplasia [10,11]. Recent studies have demonstrated that the expression of BMP-7 is decreased in acute and chronic renal diseases. Moreover, systemic administration of recombinant BMP-7 leads to repair of severely damaged renal tubular epithelial cells, in association with reversal of chronic renal injuries [12–15]. The mechanism of this action involves the reversal of epithelial-to-mesenchymal transition of tubular epithelial cells with the induction of expression of genes such as E-cadherin, a key epithelial cell adhesion molecule [15]. These actions of BMP-7 are reminiscent of the effects that this morphogen exerts during development. Collectively, BMP-7 plays critical roles in normal development of the kidney, and postnatally in repairing processes of the renal tubular damage in kidney diseases.

The indispensable roles of BMP-7 in the kidney led us to postulate that BMP antagonist(s) may modulate the renal activities of BMP-7. So far the only known BMP antagonist expressed in the kidney is gremlin [16]. Intriguingly, deletion of the *gremlin* gene in mice resulted in defects of renal morphogenesis [17]. However, although gremlin can antagonize BMP-2 and BMP-4 [18,19], the effect of gremlin on BMP-7 has not been demonstrated. These observations suggest the existence of additional BMP antagonist(s) that interfere with the actions of BMP-7 in the kidney.

Through a genome-wide search for kidney-specific human transcripts, we found a novel gene, which encodes a secretory protein with a signal peptide and cysteine-rich domain. The rat ortholog of the gene was previously reported as a gene of unknown function that was preferentially expressed in sensitized endometrium, termed uterine sensitization-associated gene-1 (USAG-1) [19]. However, its biological role and expression patterns in embryonic and adult tissues have not been described. A search of the GenBank dbEST database on the amino acid sequence of USAG-1 detected only one similar EST entry, which encodes sclerostin, a recently identified BMP antagonist expressed in bones [20,21]. This led us to speculate that USAG-1 might be a BMP antagonist expressed in the kidney. To evaluate this hypothesis, we examined whether recombinant USAG-1 antagonizes the activities of BMPs in vitro and in vivo.

Materials and methods

Plasmid construction. Human USAG-1 cDNA clone (DKFZP564D206) was purchased from Invitrogen (Carlsbad, CA) and subcloned into pCS2 vector for in vitro transcription (pCS2-hUSAG1). Human USAG-1 tagged with Flag and 6× His at its C-terminus were each cloned into pEF4 expression vector (Invitrogen) (pEF4-hUSAG1-Flag and pEF4-hUSAG1-His, respectively). We also constructed a plasmid, which includes the prolactin signal sequence followed by Flag tag [22] that was joined to USAG-1 residue 24, and a Myc tag in the C-terminus (pEF4-Flag-hUSAG1-Myc).

Cell culture and transfection. The C2C12 mouse myoblast cell line was obtained from the American Type Culture Collection. The cells were maintained in Dulbecco's modified Eagle's medium (DMEM) containing 20% fetal bovine serum (FBS) and 100 U/ml penicillin. COS-7 cells were cultured in DMEM supplemented with 10% FBS and plasmids were transfected using the LipofectAMINE reagent (Invitrogen) following manufacturer's instructions. Cells were cultured and maintained at 37 °C in a humidified atmosphere of 95% air/5% CO_2.

Western blotting. COS7 cells transfected with the designated plasmids were washed with phosphate-buffered saline (PBS) and solubilized in a buffer containing 20 mM Tris–HCl, pH 7.5, 150 mM NaCl, 1% Triton X-100, 1% aprotinin, and 1 mM phenylmethylsulfonyl fluoride. Lysates were cleared by centrifugation, applied to 15% SDS–polyacrylamide gel electrophoresis, and transferred to nitrocellulose filter (Protran) (Schleicher & Schuell, Keene, NH). Membranes were subjected to immunoblotting with the designated antibodies, followed by visualization using the Enhanced Chemiluminescence detection system (Pharmacia, Piscataway, NJ). Antibodies used were: anti-Flag M1 and M2 monoclonal antibodies (Sigma, St. Louis, MO), anti-Myc monoclonal antibody and anti-His polyclonal antibody (Santa Cruz Biotechnology, Santa Cruz, CA), and anti-BMP-2, -4, and -7 monoclonal antibodies (R&D systems, Minneapolis, MN). Rabbit polyclonal anti-USAG-1 antibody was generated by immunizing rabbits with a synthetic peptide corresponding to the N-terminal sequence of secreted USAG-1 (FKNDATEILYSHC), which was conjugated with keyhole limpet hemocyanin, using the Imject Maleimide Activate mcKLH kit (Pierce, Rockford, IL) according to the manufacturer's instructions.

Co-immunoprecipitation. Lysates of COS7 cells transfected with a pEF4 mock vector or pEF4-hUSAG1-Flag (see above) were pre-incubated with BMPs for 1 h at room temperature in 1 ml binding buffer containing 137 mM NaCl, 8.1 mM Na_2HPO_4, 2.68 mM KCl, 1.47 mM KH_2PO_4, 1 mM $CaCl_2$, 3 mM $MgCl_2$, 0.2% NP40, and 1 mg/ml BSA. After 1 h, 30 μl of anti-Flag M2 affinity gel (Sigma) was added to each reaction and incubated overnight. Gel was washed three times with 1 ml binding buffer containing 0.2% Tween 20 and subjected to immunoblotting with anti-BMP antibodies.

Preparation of culture supernatant. COS7 cells transfected with pEF4-hUSAG1-His (see above) were cultured in serum-free DMEM for 72 h, and the conditioned medium (100 ml) was concentrated to 100 μl using Centriprep YM10, Centricon YM10, and Microcon YM10 sequentially (Millipore, Bedford, MA).

Assays for alkaline phosphatase activity. BMP-2, -4, -7, and noggin-Fc fusion protein were purchased from R&D systems. C2C12 cells were plated at a density of 500 cells/well in a 96-well plate. After 24 h, C2C12 cells were stimulated with the designated BMP and indicated amounts of concentrated medium for 48 h. Cells were washed and extracted with a lysis buffer as described previously [23,24], and alkaline phosphatase activity was determined using *p*-nitrophenylphosphate (Sigma) as substrate.

Xenopus embryo manipulation and microinjection. Embryo manipulations and microinjections were performed as described previously [3]. Capped synthetic mRNA of human USAG-1 was generated by in vitro transcription of linearized templates by using the Megascript kit (Ambion, Austin, TX). mRNA was injected into the animal pole or into the marginal zone of a ventral blastomere at the four-cell stage.

Reverse transcription-PCR analysis. Total RNA was isolated from pooled (at least 15) animal caps and subjected to reverse

transcription (RT)-PCR analysis as described previously [25] by using the following conditions: 94 °C for 5 min, followed by designated numbers of cycles at 94 °C for 30 s, 55 °C for 30 s, and 72 °C for 2 min. Primers for neural cell adhesion molecule (NCAM), muscle actin, and histone H4 have been described previously [25]. PCR products were visualized by electrophoresis on agarose gels followed by ethidium bromide staining.

Northern blots. Northern blot membranes were purchased from BD Biosciences (Palo Alto, CA). Membranes were hybridized with a full-length human and mouse USAG-1 cDNA probe random-prime labeled with [^{32}P]dCTP (10 mCi/ml; Amersham, Buckinghamshire, UK).

In situ hybridization. In situ hybridization was performed as previously described [26]. The sense or anti-sense USAG-1 riboprobes were prepared using mouse USAG-1 cDNA (621 bp) as a template.

Luciferase assays. 293T cells were transfected using Lipofectamine 2000 (Invitrogen) with a total of 2 μg of various concentrations of plasmids as described [27]: 0.2 μg of pTOP-tk-luciferase reporter plasmid, 0.05 μg of internal control pRL-tk *Renilla* reporter plasmid (Promega, Madison, WI), the designated amount of Wnt1 expression vector (pCS2-mWnt1), pCS2-hUSAG1, DKK1 expression vector (pcDNA-hDKK1-Flag), and control vector (pCS2 expression vector) as stuffer. Luciferase activities were measured 24 h after transfection using the Dual-Luciferase Reporter Assay System (Promega).

Results

Primary structure of USAG-1

During a search of kidney-specific human transcripts in EST databases, we found the cDNA DKFZP564 D206. An inter-specific search for EST sequences homologous to this cDNA revealed that it is a human ortholog of the rat gene named uterine sensitization-associated gene-1 (USAG-1), which was previously reported as a transcript preferentially expressed in sensitized endometrium [19] (Fig. 1A). A mouse ortholog was also found from databases as RIKEN cDNA named 0610006G05Rik. Amino acid sequences encoded in the rat and mouse cDNAs are 97% and 98% identical to the human sequence, respectively, indicating high degrees of sequence conservation. A web-based domain prediction software (Simple Modular Architecture Research Tool: SMART) and signal peptide prediction software (SignalP) predicted this protein to be a member of the cystine-knot superfamily with an N-terminal signal peptide

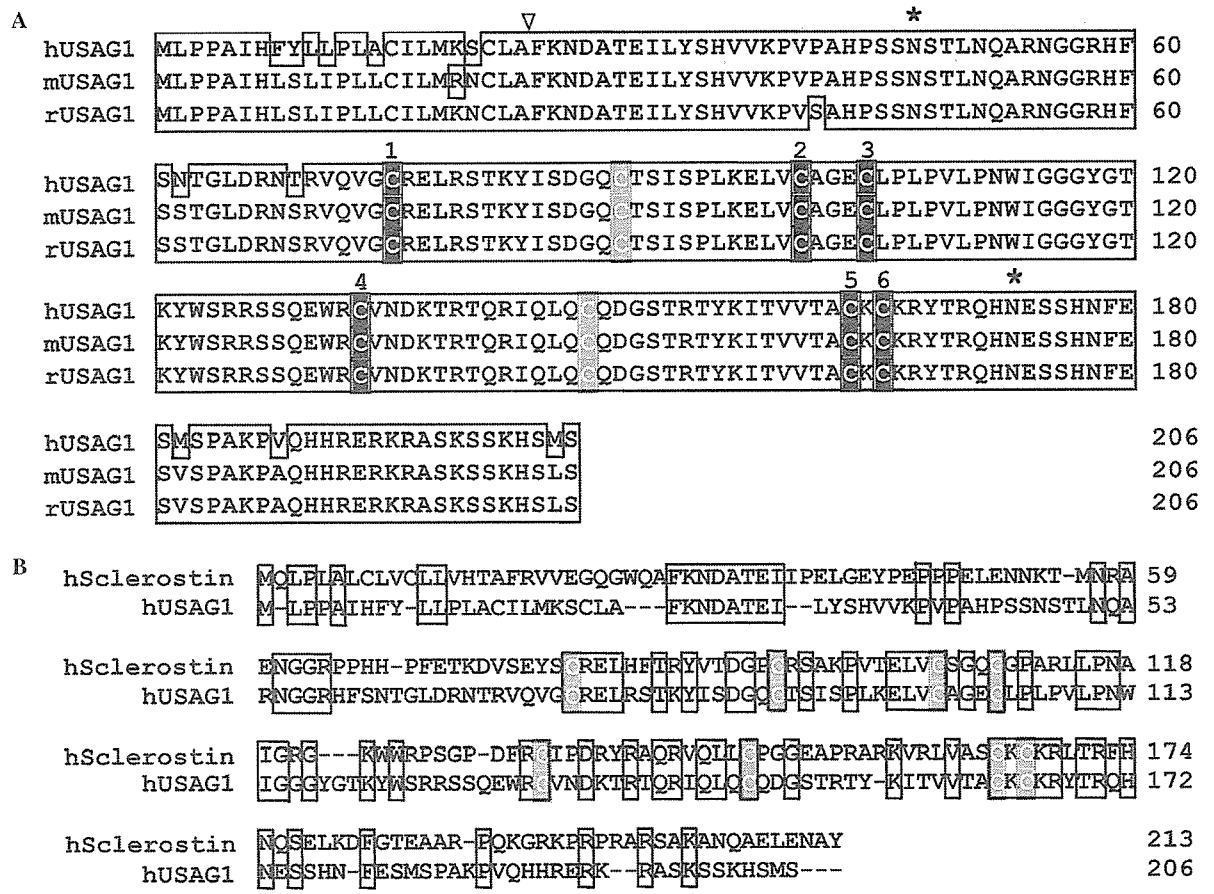

Fig. 1. Sequence alignment of USAG-1. (A) Alignment of encoded amino acid sequences of human, mouse, and rat USAG-1. Six cysteine residues (labeled 1–6) that constitute the predicted cystine-knot fold are shown in black boxes. The extra cysteine residues, conserved among species but not among other BMP antagonists, are shown in gray boxes. Residues shared by more than two species are enclosed. Putative cleavage site of signal sequence is shown by an arrowhead and potential sites for N-linked glycosylation by asterisks. (B) Alignment of human USAG-1 and human sclerostin, the *Sost* gene product. Common amino acid residues are enclosed. Note that all eight cysteine residues (shown in gray boxes) are conserved in both proteins.

of 23 amino acids. Further, homology searches revealed that USAG-1 has significant amino acid identities (38%) to sclerostin, the product of the *Sost* gene (Fig. 1B). Mutations of *Sost* are found in patients with sclerosteosis, a syndrome of sclerosing skeletal dysplasia [28]. Sclerostin is subsequently shown to be a new member of BMP antagonist expressed in bones and cartilages [20,21]. We therefore postulated that USAG-1 might be a BMP antagonist expressed in the kidney.

Secreted form of human USAG-1

To examine whether USAG-1 is a secreted protein, the culture medium of COS7 cells transfected with a mock vector or the pEF4-hUSAG1-His expression plasmid (see Materials and methods) was subjected to immunoblotting (Fig. 2A). Two major bands with apparent molecular masses of 28–30 kDa were detected only in the culture medium of COS7 cells transfected with pEF4-hUSAG1-His, showing that the His-tagged USAG-1 was indeed secreted. The observed molecular masses on SDS–PAGE were higher than the calculated mass of recombinant USAG-1 (20.1 kDa). The USAG-1 sequence contains possible N-glycosylation sites at conserved Asn47 and Asn173 (Fig. 1A), and the shift of molecular mass may be due to glycosylation at these sites. The two major bands of USAG-1 might also be due to heterogeneity of glycosylation.

Since a number of BMP antagonists, such as noggin and DAN, are known to form disulfide-bridged dimers [29], we next examined whether USAG-1 also forms a dimer. Because tags at the C-terminus might interfere with the formation of dimers, we transfected COS7 cells with native form of human USAG-1 (pCS2-hUSAG1; see Materials and methods) and the lysates were subjected to immunoblotting with anti-USAG-1 antibody raised against an N-terminal sequence of USAG-1 after the signal peptide. USAG-1 contained in the lysates of COS7 cells transfected with pCS2-hUSAG1 exhibited essentially the same apparent molecular mass under non-reducing and reducing conditions (Fig. 2B). Similar results were obtained with concentrated culture medium of COS7 cells transfected with pCS2-hUSAG1, indicating that human USAG-1 was secreted as a monomer (data not shown). This is consistent with the fact that USAG-1 does not have the extra cysteine residues present in noggin and DAN, which are necessary to make inter-molecular disulfide bridges.

To examine whether the N- or C-terminus of USAG-1 protein is proteolytically processed, several constructs

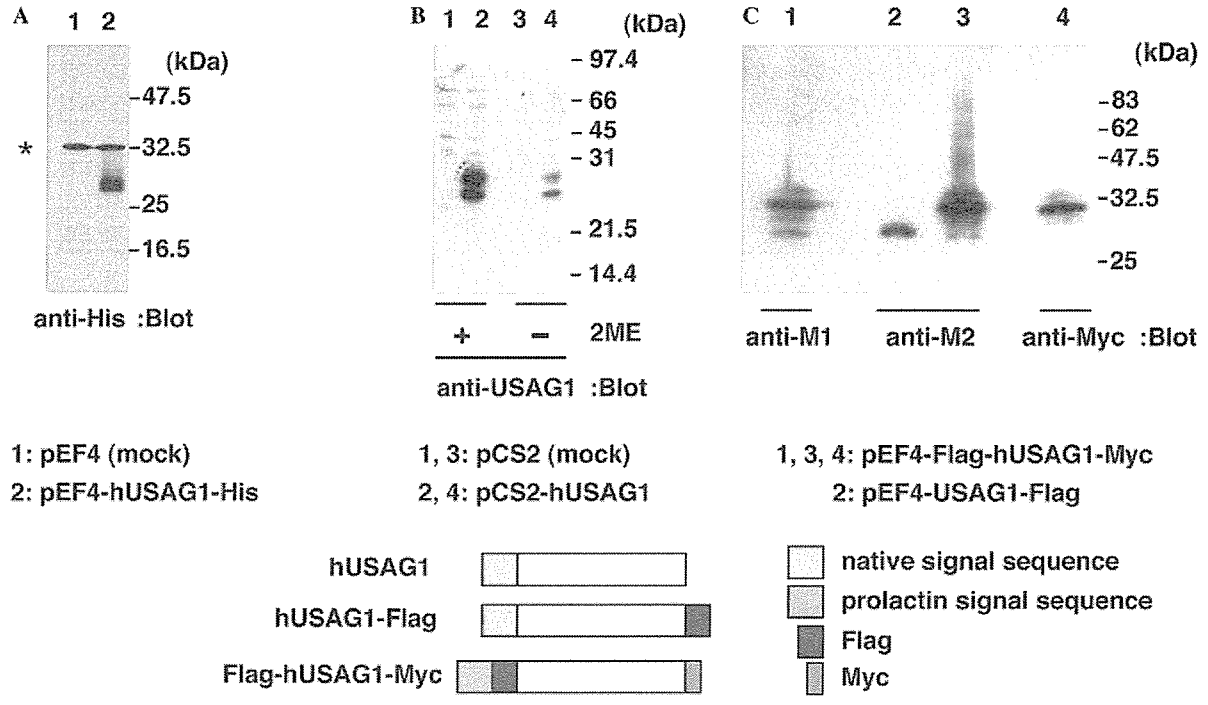

Fig. 2. Secretion of recombinant human USAG-1. (A) Culture supernatant from COS7 cells transfected with pEF4 mock vector (lane 1) or pEF4-hUSAG1-His (lane 2) was subjected to immunoblotting with anti-His antibody. Representative data from three independent experiments are shown. Non-specific signals are indicated by asterisks. (B) Lysates of COS7 cells transfected with pCS2 mock vector (lanes 1 and 3) and pCS2-hUSAG1 (lanes 2 and 4) separated by SDS–polyacrylamide gel electrophoresis under reducing (with 2-mercaptoethanol) (lanes 1 and 2) or non-reducing (without 2ME) (lanes 3 and 4) conditions were subjected to immunoblotting with anti-USAG-1 antibody. Representative data are shown from three independent experiments. (C) Lysates of COS7 cells transfected with pEF4-Flag-hUSAG1-Myc (lanes 1, 3, and 4) and pEF4-hUSAG1-Flag (lane 2) were subjected to immunoblotting with anti-Flag M1 (lane 1), anti-Flag M2 (lanes 2 and 3), and anti-Myc (lane 4) antibodies. Representative data are shown from three independent experiments.

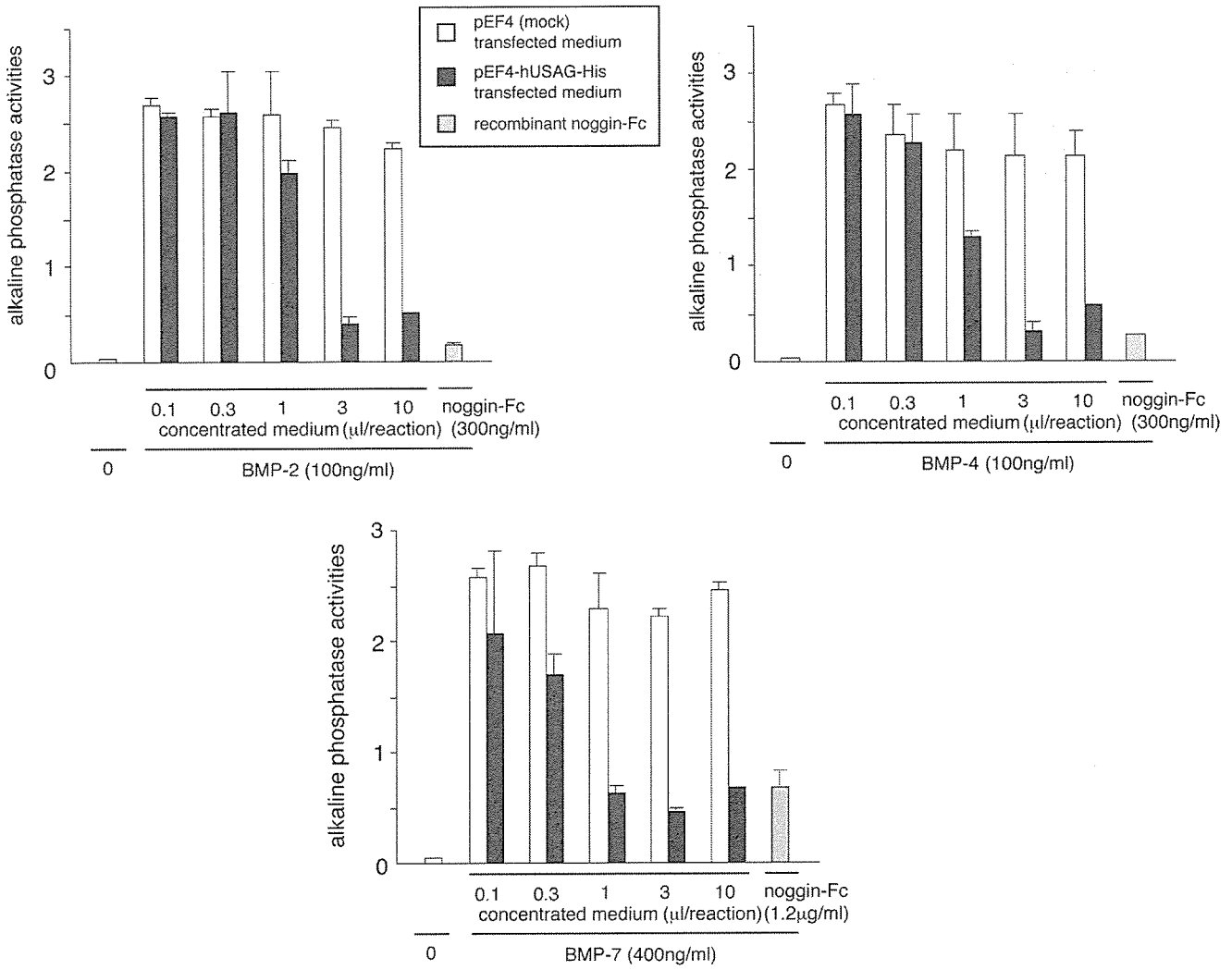

Fig. 3. Effects of USAG-1 on BMP-induced alkaline phosphatase activity in C2C12 cells. C2C12 cells were treated for 48 h with BMP-2 (100 ng/ml), BMP-4 (100 ng/ml) or BMP-7 (400 ng/ml), plus the indicated doses of concentrated culture medium from COS7 cells transfected with pEF4 mock vector (white bars) or pEF4-hUSAG1-His (black bars). Indicated doses of noggin-Fc were used as positive controls (gray bars). After treatment, cellular alkaline phosphatase activity was determined. Results are means ± SD for quadruplicate cultures. Representative data are shown from three separate experiments.

with different tags at its either terminus were expressed in COS7 cells. In the lysate of COS7 cells transfected with pEF4-USAG1-Flag (see Materials and methods), expressed protein is detectable with the anti-Flag M2 antibody (Fig. 2C), indicating that the tagged C-terminus of USAG-1 was not cleaved posttranslationally. In the lysates of COS7 cells transfected with pEF4-Flag-USAG1-Myc (see Materials and methods), protein was detectable either with the anti-Flag M1, anti-Flag M2 or anti-Myc antibody. Similar results were obtained with concentrated culture medium from these cells (data not shown), indicating that neither terminus of USAG-1 is cleaved during the transit through the secretory pathway.

USAG-1 antagonizes the action of BMPs in C2C12 cells

To determine whether USAG-1 can act as a BMP antagonist, we first examined the effects of USAG-1 on the activity of BMP-2, BMP-4, and BMP-7 inducing differentiation of C2C12 cells by measuring the alkaline phosphatase activity. BMP-2, -4, and -7 markedly stimulated the alkaline phosphatase activity in C2C12 cells as previously reported [23,24] (Fig. 3). Addition of culture supernatant from pEF4-USAG1-His-transfected COS7 cells inhibited BMP-2, -4 or -7-induced alkaline phosphatase activities in a dose-dependent manner, while addition of conditioned medium of mock transfected COS7 cells exerted no appreciable effects.

USAG-1 inhibits endogenous BMP activity in Xenopus embryogenesis

Next we examined whether USAG-1 antagonizes BMP activities in vivo in *Xenopus* embryos. Ventral injection of synthetic mRNA encoding a BMP antagonist is known to induce secondary axis and hyperdorsaliza-

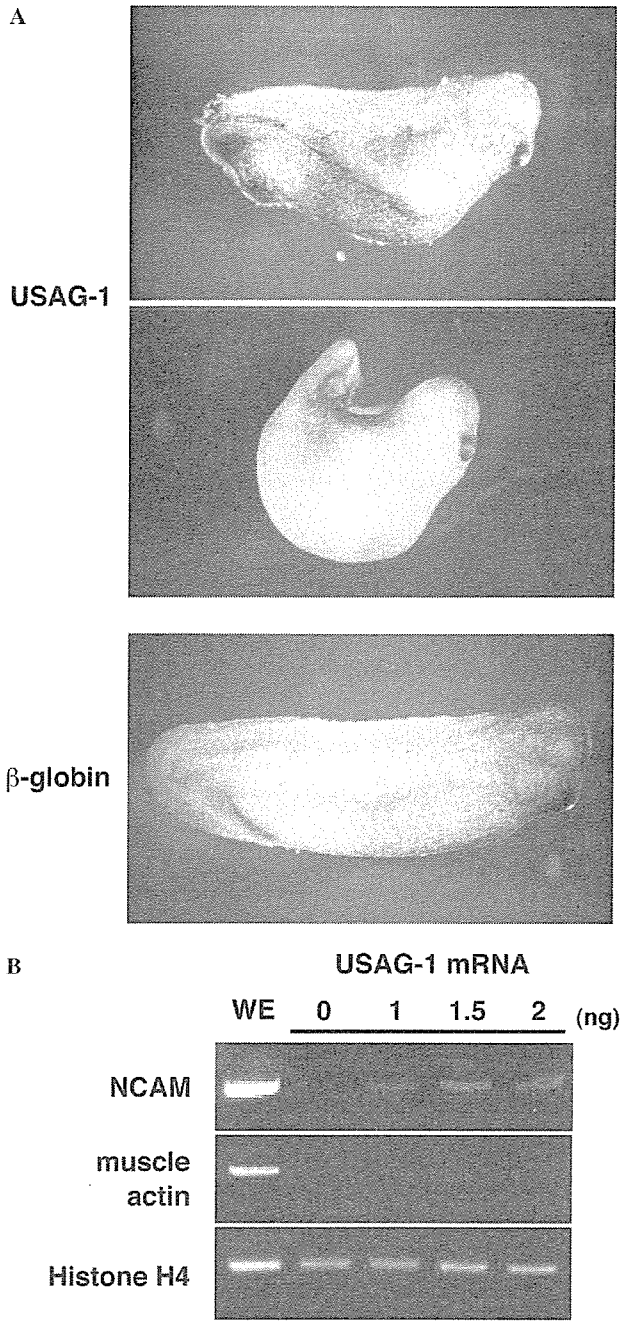

Fig. 4. USAG-1 inhibits endogenous BMP signaling in *Xenopus* embryos. (A) USAG-1 RNA (0.5 ng) was injected near the ventral midline of four-cell embryos. Typical resultant phenotypes are shown (top panel, secondary axis; middle panel, hyperdorsalized embryo). When 1 ng of β-globin RNA was injected, embryos developed normally (bottom panel). (B) Increasing doses of RNA encoding USAG-1 were injected near the animal pole of two-cell embryos. Animal caps were isolated from embryos at blastula stage 8 and cultured to stage 23. Total RNA was extracted from pooled caps and control embryos, and subjected to RT-PCR analysis. WE, whole embryo. Representative data are shown from three independent experiments.

tion in *Xenopus* embryos by blocking the ventralizing signal of BMPs [30]. We found that the injection of low doses of synthetic USAG-1 mRNA caused secondary axis formation and hyperdorsalized phenotype, in which the trunk and tail were severely reduced or lost (Fig. 4A, top and middle panels). In contrast, embryos developed normally when irrelevant mRNA (encoding β-globin) was injected (Fig. 4A, bottom). Injection of as little as 100 pg USAG-1 mRNA was sufficient to cause secondary axis formation, and injection of increasing doses of mRNA up to 1000 pg led to a corresponding increase in the frequency of secondary axis formation and hyperdorsalization (Table 1).

Table 1
The effects of USAG-1 on the formation of dorsalized phenotypes

Injected RNA (pg)		Dorsalized phenoptypes (%)			*N*
USAG-1	β-Globin	Hyperdorsalization	Secondary axis	Total	
0	0	0	0	0	50
0	500	0	0	0	28
0	1000	0	0	0	36
100	0	14	25	39	28
200	0	18	45	63	33
500	0	30	40	70	40
1000	0	41	36	77	56

Although these effects strongly suggest that USAG-1 acts as a BMP antagonist in vivo, it is known that similar effects are also observed when the activin signaling pathway is stimulated in *Xenopus* embryos [25]. Overexpression of activin induces the formation of mesoderm including Spemann organizer, and the induction of the organizer in turn forces dorsalization of *Xenopus* embryos. To determine whether the dorsalization phenotype we observed above represents a direct effect of inhibition of BMP signaling, or it is a consequence of mesodermal induction by activin signaling, we next examined the activities of USAG-1 mRNA on *Xenopus* animal-cap explants. Injection of mRNA for a BMP antagonist into the animal pole of *Xenopus* embryos induces neural differentiation of explants, as evidenced by the expression of neural markers such as NCAM [31,32], whereas the injection of activin is known to induce mesodermal markers such as muscle actin [25]. Injection of USAG-1 mRNA induced expression of NCAM in animal caps dose-dependently, but not that of muscle actin (Fig. 4B). These results indicate that USAG-1 directly antagonizes BMP signaling in *Xenopus* embryos.

USAG-1 directly binds BMP-2, -4, and -7

Since many BMP antagonists are known to physically bind BMPs to neutralize their activities, we examined whether USAG-1 binds directly to BMP proteins by co-immunoprecipitation. Lysates of COS7 cells transfected with pEF4 mock vector or pEF4-hUSAG1-Flag (see Materials and methods) were incubated with the anti-Flag M2 affinity gel in the presence or absence of

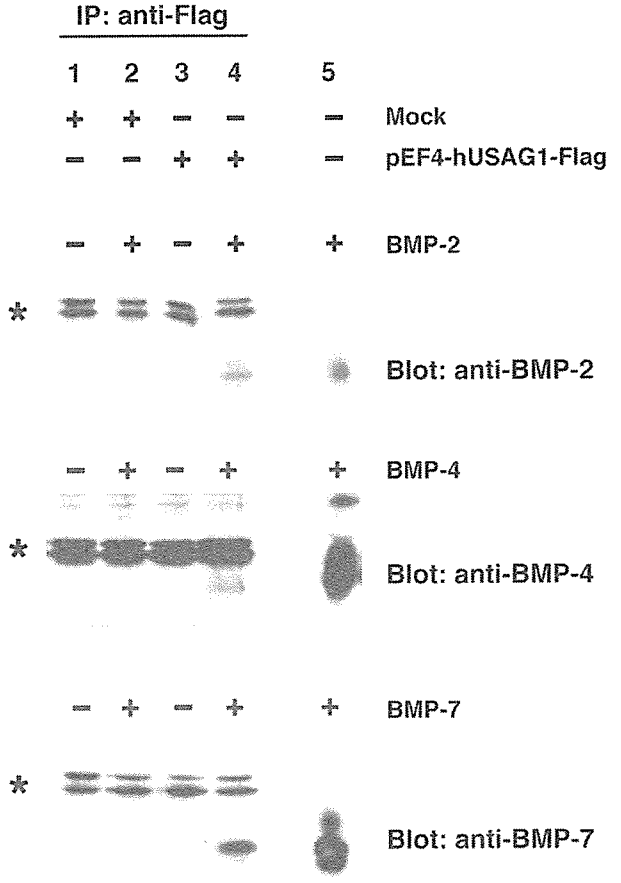

Fig. 5. USAG-1 binds BMP-2, -4, and -7. Lysates of COS7 cells transfected with pEF4 mock vector (lanes 1 and 2) and pEF4-hUSAG1-Flag (lanes 3 and 4) were incubated with anti-Flag M2 antibody affinity gel in the presence (lanes 2 and 4) or absence (lanes 1 and 3) of BMP (450 ng). Gel was washed and subjected to immunoblotting with anti-BMP antibodies. Lane 5 shows the positive control for immunoblotting of BMP-2, -4, and -7 (50 ng/lane). Representative data are shown from three independent experiments.

recombinant BMP proteins. Gel was washed and subjected to immunoblotting with anti-BMP antibodies. We detected BMP-2, -4, and -7 co-precipitated with USAG-1-Flag, demonstrating that USAG-1 physically associates with these BMP proteins (Fig. 5).

Tissue distribution of USAG-1 in fetal and adult mice

Because USAG-1 inhibits the dorsalizing activities of BMPs in *Xenopus* embryos, we postulated that USAG-1 might play roles in embryogenesis and we examined the expression of USAG-1 in mouse embryos. Expression of USAG-1 mRNA was first detected on embryonic Day 11 (E11) in the whole mouse embryo and increased towards E17 (Fig. 6A). In situ hybridization to mouse embryos showed that, on E11.5, USAG-1 mRNA was expressed in several tissues including the first and second branchial arches, pharynx, and metanephros (Figs. 7A–C). On E17.5, strong USAG-1 mRNA expression was restricted to kidney tubules and ameloblasts in teeth

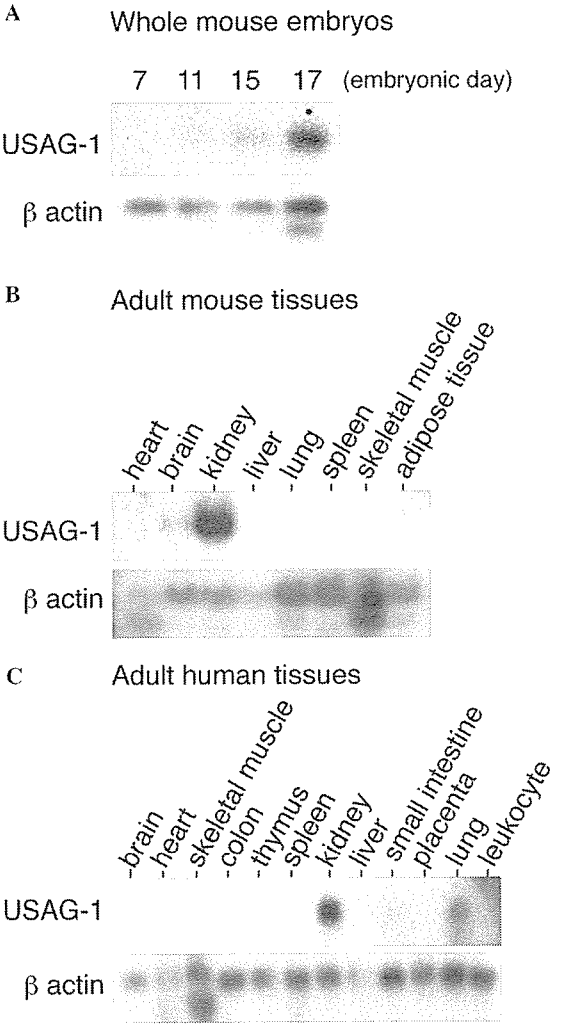

Fig. 6. Tissue distribution of USAG-1 mRNA. (A) Northern blot analysis of mouse whole embryos with embryonic day noted above each lane. (B,C) Northern blots of mouse (B) and human (C) tissues. Lower panels, membranes were re-hybridized with β-actin probe as internal control.

(Figs. 7D–F). In addition, moderate expression was observed in hair follicles (Fig. 7G), choroids plexus of the fourth cerebral ventricle (Fig. 7H), and ependymal cells in the lateral ventricle of the brain (Fig. 7I).

We also examined the distribution of USAG-1 mRNA in adult tissues. The expression was by far most abundant in the kidney, as shown by multi-tissue Northern blots of mice and humans (Figs. 6B and C). Weak expression was observed in the mouse brain and human lung. In situ hybridization to sections of adult mouse kidneys revealed a highly localized expression in the distal tubules (Figs. 7J–L). No expression was observed in glomeruli or blood vessels in the kidney.

Effects of USAG-1 on Wnt1 signaling

While the present study was being carried out, a *Xenopus* ortholog of USAG-1 (termed Wise) was

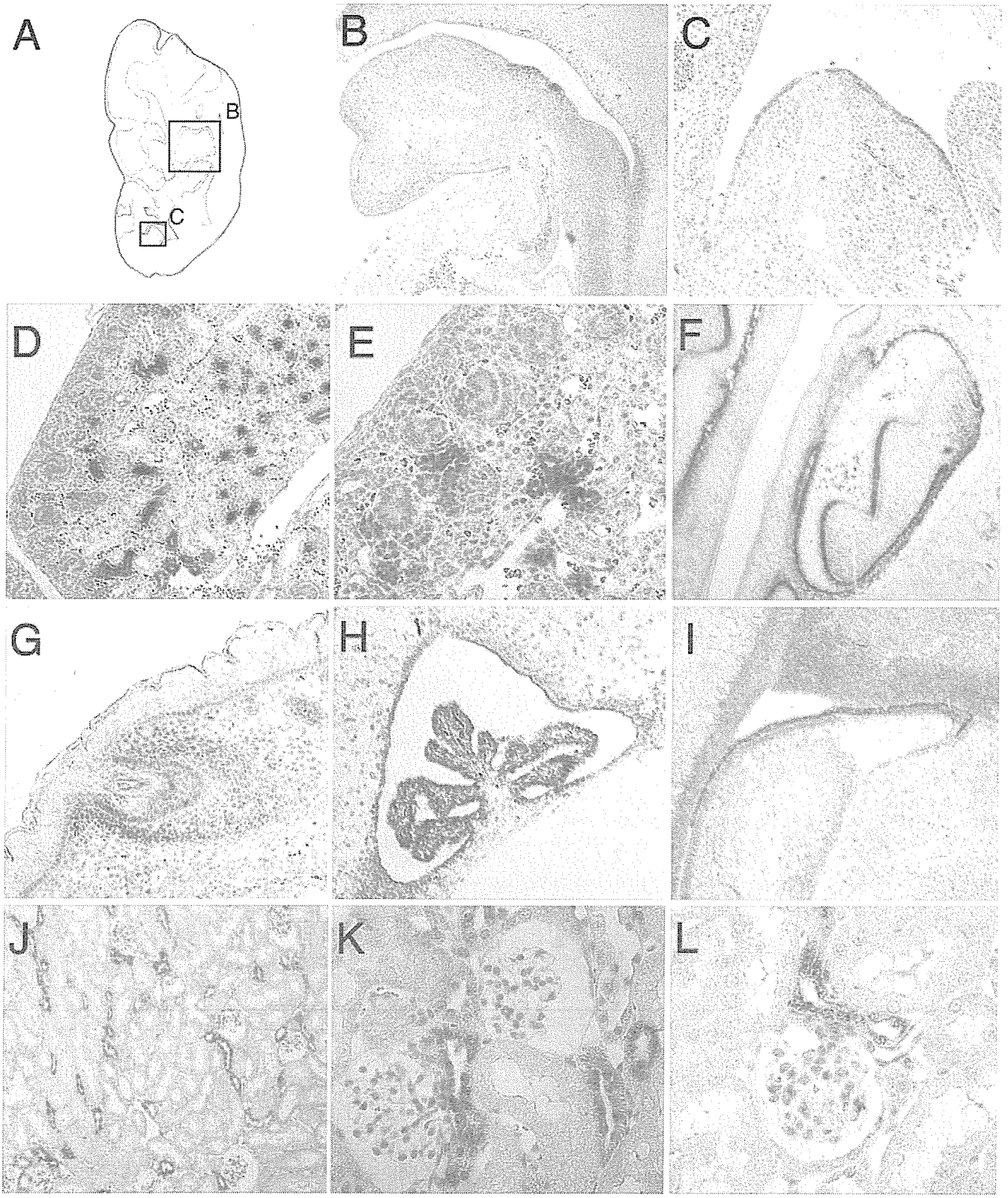

Fig. 7. In situ hybridization of mouse USAG-1 mRNA. (A) Schematic drawing of sagittal section of E11.5 mouse embryo, showing the approximate fields for (B) and (C). (B) USAG-1 is expressed in the first and second branchial arches and in pharynx at E11.5. (C) USAG-1 is also expressed in metanephros. In E17.5 mouse embryos, the expression of USAG-1 is prominent in kidney tubules [(D) lower magnification, (E) higher magnification], and in ameloblasts of teeth (F). Moderate expression is observed in hair follicles (G), choroids plexus in the fourth brain ventricle (H), and in ependymal cells of the lateral ventricle (I). In adult kidney, the expression of USAG-1 is confined to distal tubules [(J) lower magnification, (K,L) higher magnification].

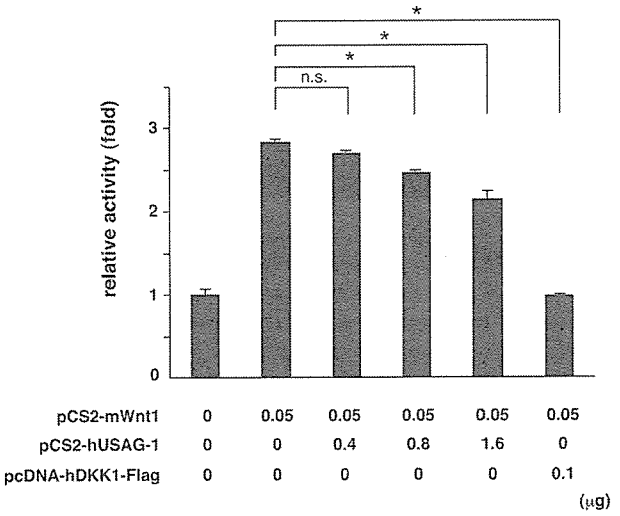

Fig. 8. Effect of USAG-1 on Wnt-1-induced β-catenin/TCF-regulated transcription. 293T cells were transfected with pTOP-tk-luciferase reporter plasmid and pRL-tk *Renilla* reporter plasmid, plus pCS2-hUSAG1, pCS2-mWnt1, and/or pcDNA-hDKK1-Flag as designated. Luciferase activities were measured after 24 h and expressed relative to the samples not transfected with pCS2-mWnt1. Results are means ± SD for triplicate wells. Representative data are shown from three independent experiments. $^*P < .0001$; n.s., not significant; by Fisher's PLSD.

reported to function as a context-dependent activator and inhibitor of Wnt signaling by directly binding LRP6 [33]. Therefore, we examined the possible effect of human USAG-1 on the Wnt1-induced β-catenin/TCF-regulated transcription, using a luciferase reporter assay as described previously [27]. Co-transfection of pCS2-hUSAG1 slightly but dose-dependently inhibited the luciferase activities induced by Wnt1. However, the effect of USAG1 was considerably weaker compared to that of the canonical Wnt antagonist DKK1 (Fig. 8).

Discussion

In this study, we have shown at the cellular and organismal levels that USAG-1 inhibits BMP actions. We have found that the expression of USAG-1 mRNA increases towards the late stage of mouse embryogenesis, and it is primarily confined to distal tubules of the kidney in adult mice. Avsian-Kretchmer and Hsueh [34] very recently reported the human ortholog of USAG-1 in their genome-wide search for cystine-knot proteins. Based on the sequence homology to sclerostin [20], they suggested the possibility that USAG-1 is a BMP antagonist. Our present results are consistent with their hypothesis and define USAG-1 as a novel BMP antagonist in the kidney. Furthermore, during the preparation of the present manuscript, Laurikkala et al. [35] independently reported that the mouse and human ortholog of USAG-1 (termed Ectodin) acts as a BMP antagonist in tooth enamel knot. Our present observations are also consistent with their results. The primary structures of USAG-1 and sclerostin are rather dissimilar to other known BMP antagonists. USAG-1 and sclerostin are secreted as monomers, while many other BMP antagonists form dimers. The expression of USAG-1 and sclerostin is also relatively confined to a certain tissue, i.e., USAG-1 in the kidney and sclerostin in bones, whereas other BMP antagonists tend to be widely expressed in many tissues. We thus propose that USAG-1 and sclerostin represent a distinct family of tissue-specific BMP antagonists.

The expression of USAG-1 mRNA in adult mouse kidney is restricted to the epithelial cells of distal collecting tubules. Previous studies showed the expression of BMP-7 in the tubular epithelial cells of all segments, although staining was most intense in distal convoluted tubules and collecting ducts [36]. The type II receptor for BMP-7 is expressed in the renal cortex as well as in the medulla, though the injection of radiolabeled BMP-7 revealed that majority of labeled BMP-7 accumulated in glomeruli and the adjacent distal convoluted tubules [37]. Thus, the cellular distribution of BMP-7 and its receptor is partially overlapping with that of USAG-1; it is attractive to speculate that USAG-1 interacts with BMP-7 in the distal convoluted tubules to modulate the local BMP functions.

Our preliminary studies have shown that renal expression of USAG-1 is upregulated in disease models such as nephrosclerosis in Dahl salt-sensitive hypertensive rats (data not shown). It has been shown that renal expression of BMP-7 is reduced in acute and chronic renal injuries, and the reduction plays an important role in progression of the disease [36]. Therefore, we speculate that increased expression of USAG-1 in these pathological situations might inhibit the actions of remaining BMP-7 available and may further worsen the injuries to kidney tubules.

In embryogenesis, BMP-7 has an essential role in metanephric development [10,11,38]. Analysis of *BMP-7* null mice has shown that BMP-7 expression is required for coordinating the branching morphogenesis of the ureteric bud and for renal epithelium formation from condensing mesenchyme [10,11]. USAG-1 mRNA in the metanephros at E11.5 is confined to the epithelial lining (Fig. 7C), while BMP-7 is expressed in the ureteric bud and the surrounding mesenchymal condensates [39]. BMP-4, also known to play a role in kidney organogenesis, is expressed in the mesenchymal cells surrounding the Wolffian duct but not in the metanephric mesenchyme at E10.5 [40]. Therefore, the spatial pattern of USAG-1 expression in these embryonic stages is not closely overlapping with that of BMPs, and the possible role of USAG-1 in the early renal organogenesis remains to be determined. However, in the later stage of renal development, both USAG-1 and BMP-7 localize within the tubules, suggesting the possibility that USAG-1 interferes with the activities of BMP-7 there. Precise

evaluation of USAG-1 expression through developmental stages will provide further insights into the interaction between USAG-1 and BMPs in kidney organogenesis.

Among the known BMP antagonists, Gremlin is also expressed in the kidney [16] and has been considered to play a role in the progression of certain kidney diseases [41]. However, there are important differences between Gremlin and USAG-1: first, target molecules of Gremlin are considered to be BMP-2 and BMP-4 [18], whereas USAG-1 antagonizes BMP-7 as well. Second, Gremlin is expressed in mesangial cells in the glomerulus [16], while USAG-1 is expressed in epithelial cells of distal tubules. Finally, according to phylogenetic analyses [34], the distance between Gremlin and USAG-1 is considerably far. We speculate that these two BMP antagonists play distinct roles in the development and progression of kidney diseases.

In later developmental stages, USAG-1 is highly expressed also in ameloblasts of teeth. Ameloblasts secrete enamel matrix extracts, of which the mineralization remains incomplete until apathetic crystals accumulate [42]. It has recently been reported that BMPs in enamel extracts induce mineralization of teeth and exogenous administration of recombinant noggin inhibits these activities in tissue cultures [43]. Thus far, however, no endogenous BMP antagonist has been described in developing tooth tissues. We postulate that USAG-1 secreted from ameloblasts may modulate the activities of BMPs and regulate mineralization of enamel matrix extracts. Indeed, a very recent report seems to support this hypothesis [35].

USAG-1 is also expressed in hair follicles of E17.5 mouse embryos. It has been reported that noggin is expressed in hair follicles and plays a critical role in the induction of hair follicle by modulating the activities of BMPs [44,45]. USAG-1 might also share some roles with noggin in hair follicle induction.

Rat USAG-1 was originally reported as a gene preferentially expressed in the receptive rat endometrium [19]. We examined the expression of USAG-1 mRNA in the uterus of 6-week-old female Wistar rats at random, without synchronizing their stage of estrous cycle (data not shown). The levels of expression in the uterus varied from undetectable to almost comparable to the levels in the kidney, probably depending on the estrous cycle.

In partial disagreement with a recent report on the *Xenopus* homolog of USAG-1 [33], we have found in the present study that human USAG-1 inhibits the Wnt1 action in a TCF-mediated transcriptional reporter assay only slightly, an effect considerably weaker than that of the established Wnt antagonist DKK1 in the same assay. Close relationships between the Wnt and BMP pathways have been recently reported: for instance, noggin and DKK1 cooperate in head induction [46], while the expression of DKK1 is regulated by BMP-4 in limb development [47]. Furthermore, a BMP antagonist called Cerberus has a binding site for Wnt proteins that is distinct from the BMP binding site, and antagonizes Wnt activities by directly binding Wnt [48]. The effect of USAG-1 on the Wnt pathway requires further investigation.

Acknowledgments

We thank I. Charo for prolactin-Flag-CCR2 plasmid and T. Imamura for advice on alkaline phosphatase assays. M.Y. is an Investigator of the Howard Hughes Medical Institute. This work was supported in part by the Exploratory Research for Advanced Technology (Yanagisawa Orphan Receptor Project) of the Japan Science and Technology Agency.

References

[1] J. Massague, Y.G. Chen, Controlling TGF-beta signaling, Genes Dev. 14 (2000) 627–644.
[2] B.L. Hogan, Bone morphogenetic proteins: multifunctional regulators of vertebrate development, Genes Dev. 10 (1996) 1580–1594.
[3] G. Murakami, T. Watabe, K. Takaoka, K. Miyazono, T. Imamura, Cooperative inhibition of bone morphogenetic protein signaling by Smurf1 and inhibitory Smads, Mol. Biol. Cell 14 (2003) 2809–2817.
[4] A. Nishihara, T. Watabe, T. Imamura, K. Miyazono, Functional heterogeneity of bone morphogenetic protein receptor-II mutants found in patients with primary pulmonary hypertension, Mol. Biol. Cell 13 (2002) 3055–3063.
[5] S.J. Butler, J. Dodd, A role for BMP heterodimers in roof plate-mediated repulsion of commissural axons, Neuron 38 (2003) 389–401.
[6] S.D. Podos, K.K. Hanson, Y.C. Wang, E.L. Ferguson, The DSmurf ubiquitin–protein ligase restricts BMP signaling spatially and temporally during *Drosophila* embryogenesis, Dev. Cell 1 (2001) 567–578.
[7] J. Groppe, J. Greenwald, E. Wiater, J. Rodriguez-Leon, A.N. Economides, W. Kwiatkowski, M. Affolter, W.W. Vale, J.C. Belmonte, S. Choe, Structural basis of BMP signalling inhibition by the cystine knot protein Noggin, Nature 420 (2002) 636–642.
[8] S. Piccolo, Y. Sasai, B. Lu, E.M. De Robertis, Dorsoventral patterning in *Xenopus*: inhibition of ventral signals by direct binding of chordin to BMP-4, Cell 86 (1996) 589–598.
[9] L.B. Zimmerman, J.M. De Jesus-Escobar, R.M. Harland, The Spemann organizer signal noggin binds and inactivates bone morphogenetic protein 4, Cell 86 (1996) 599–606.
[10] A.T. Dudley, K.M. Lyons, E.J. Robertson, A requirement for bone morphogenetic protein-7 during development of the mammalian kidney and eye, Genes Dev. 9 (1995) 2795–2807.
[11] G. Luo, C. Hofmann, A.L. Bronckers, M. Sohocki, A. Bradley, G. Karsenty, BMP-7 is an inducer of nephrogenesis, and is also required for eye development and skeletal patterning, Genes Dev. 9 (1995) 2808–2820.
[12] S. Vukicevic, V. Basic, D. Rogic, N. Basic, M.S. Shih, A. Shepard, D. Jin, B. Dattatreyamurty, W. Jones, H. Dorai, S. Ryan, D. Griffiths, J. Maliakal, M. Jelic, M. Pastorcic, A. Stavljenic, T.K. Sampath, Osteogenic protein-1 (bone morphogenetic protein-7) reduces severity of injury after ischemic acute renal failure in rat, J. Clin. Invest. 102 (1998) 202–214.
[13] J. Morrissey, K. Hruska, G. Guo, S. Wang, Q. Chen, S. Klahr, Bone morphogenetic protein-7 improves renal fibrosis and accelerates the return of renal function, J. Am. Soc. Nephrol. 13 (Suppl. 1) (2002) S14–S21.

[14] S. Wang, Q. Chen, T.C. Simon, F. Strebeck, L. Chaudhary, J. Morrissey, H. Liapis, S. Klahr, K.A. Hruska, Bone morphogenic protein-7 (BMP-7), a novel therapy for diabetic nephropathy, Kidney Int. 63 (2003) 2037–2049.
[15] M. Zeisberg, J. Hanai, H. Sugimoto, T. Mammoto, D. Charytan, F. Strutz, R. Kalluri, BMP-7 counteracts TGF-beta1-induced epithelial-to-mesenchymal transition and reverses chronic renal injury, Nat. Med. 9 (2003) 964–968.
[16] R. McMahon, M. Murphy, M. Clarkson, M. Taal, H.S. Mackenzie, C. Godson, F. Martin, H.R. Brady, IHG-2, a mesangial cell gene induced by high glucose, is human gremlin. Regulation by extracellular glucose concentration, cyclic mechanical strain, and transforming growth factor-beta1, J. Biol. Chem. 275 (2000) 9901–9904.
[17] M.K. Khokha, D. Hsu, L.J. Brunet, M.S. Dionne, R.M. Harland, Gremlin is the BMP antagonist required for maintenance of Shh and Fgf signals during limb patterning, Nat. Genet. 34 (2003) 303–307.
[18] D.R. Hsu, A.N. Economides, X. Wang, P.M. Eimon, R.M. Harland, The *Xenopus* dorsalizing factor Gremlin identifies a novel family of secreted proteins that antagonize BMP activities, Mol. Cell 1 (1998) 673–683.
[19] D.G. Simmons, T.G. Kennedy, Uterine sensitization-associated gene-1: a novel gene induced within the rat endometrium at the time of uterine receptivity/sensitization for the decidual cell reaction, Biol. Reprod. 67 (2002) 1638–1645.
[20] N. Kusu, J. Laurikkala, M. Imanishi, H. Usui, M. Konishi, A. Miyake, I. Thesleff, N. Itoh, Sclerostin is a novel secreted osteoclast-derived bone morphogenetic protein antagonist with unique ligand specificity, J. Biol. Chem. 278 (2003) 24113–24117.
[21] D.G. Winkler, M.K. Sutherland, J.C. Geoghegan, C. Yu, T. Hayes, J.E. Skonier, D. Shpektor, M. Jonas, B.R. Kovacevich, K. Staehling-Hampton, M. Appleby, M.E. Brunkow, J.A. Latham, Osteocyte control of bone formation via sclerostin, a novel BMP antagonist, EMBO J. 22 (2003) 6267–6276.
[22] H. Arai, F.S. Monteclaro, C.L. Tsou, C. Franci, I.F. Charo, Dissociation of chemotaxis from agonist-induced receptor internalization in a lymphocyte cell line transfected with CCR2B. Evidence that directed migration does not require rapid modulation of signaling at the receptor level, J. Biol. Chem. 272 (1997) 25037–25042.
[23] I. Asahina, T.K. Sampath, I. Nishimura, P.V. Hauschka, Human osteogenic protein-1 induces both chondroblastic and osteoblastic differentiation of osteoprogenitor cells derived from newborn rat calvaria, J. Cell Biol. 123 (1993) 921–933.
[24] H. Nishitoh, H. Ichijo, M. Kimura, T. Matsumoto, F. Makishima, A. Yamaguchi, H. Yamashita, S. Enomoto, K. Miyazono, Identification of type I and type II serine/threonine kinase receptors for growth/differentiation factor-5, J. Biol. Chem. 271 (1996) 21345–21352.
[25] T. Nakayama, M.A. Snyder, S.S. Grewal, K. Tsuneizumi, T. Tabata, J.L. Christian, *Xenopus* Smad8 acts downstream of BMP-4 to modulate its activity during vertebrate embryonic patterning, Development 125 (1998) 857–867.
[26] M. Hoshino, M. Sone, M. Fukata, S. Kuroda, K. Kaibuchi, Y. Nabeshima, C. Hama, Identification of the stef gene that encodes a novel guanine nucleotide exchange factor specific for Racl, J. Biol. Chem. 274 (1999) 17837–17844.
[27] K. Tago, T. Nakamura, M. Nishita, J. Hyodo, S. Nagai, Y. Murata, S. Adachi, S. Ohwada, Y. Morishita, H. Shibuya, T. Akiyama, Inhibition of Wnt signaling by ICAT, a novel beta-catenin-interacting protein, Genes Dev. 14 (2000) 1741–1749.
[28] M.E. Brunkow, J.C. Gardner, J. Van Ness, B.W. Paeper, B.R. Kovacevich, S. Proll, J.E. Skonier, L. Zhao, P.J. Sabo, Y. Fu, R.S. Alisch, L. Gillett, T. Colbert, P. Tacconi, D. Galas, H. Hamersma, P. Beighton, J. Mulligan, Bone dysplasia sclerosteosis results from loss of the SOST gene product, a novel cystine knot-containing protein, Am. J. Hum. Genet. 68 (2001) 577–589.
[29] J. Groppe, J. Greenwald, E. Wiater, J. Rodriguez-Leon, A.N. Economides, W. Kwiatkowski, K. Baban, M. Affolter, W.W. Vale, J.C. Belmonte, S. Choe, Structural basis of BMP signaling inhibition by Noggin, a novel twelve-membered cystine knot protein, J. Bone Joint Surg. Am. A 85 (Suppl. 3) (2003) 52–58.
[30] R. Harland, J. Gerhart, Formation and function of Spemann's organizer, Annu. Rev. Cell Dev. Biol. 13 (1997) 611–667.
[31] C.R. Kintner, D.A. Melton, Expression of *Xenopus* N-CAM RNA in ectoderm is an early response to neural induction, Development 99 (1987) 311–325.
[32] T. Bouwmeester, S. Kim, Y. Sasai, B. Lu, E.M. De Robertis, Cerberus is a head-inducing secreted factor expressed in the anterior endoderm of Spemann's organizer, Nature 382 (1996) 595–601.
[33] N. Itasaki, C.M. Jones, S. Mercurio, A. Rowe, P.M. Domingos, J.C. Smith, R. Krumlauf, Wise, a context-dependent activator and inhibitor of Wnt signalling, Development 130 (2003) 4295–4305.
[34] O. Avsian-Kretchmer, A.J. Hsueh, Comparative genomic analysis of the eight-membered-ring cystine-knot-containing bone morphogenetic protein (BMP) antagonists, Mol. Endocrinol. (2003).
[35] J. Laurikkala, Y. Kassai, L. Pakkasjarvi, I. Thesleff, N. Itoh, Identification of a secreted BMP antagonist, ectodin, integrating BMP, FGF, and SHH signals from the tooth enamel knot, Dev. Biol. 264 (2003) 91–105.
[36] S.N. Wang, J. Lapage, R. Hirschberg, Loss of tubular bone morphogenetic protein-7 in diabetic nephropathy, J. Am. Soc. Nephrol. 12 (2001) 2392–2399.
[37] D. Bosukonda, M.S. Shih, K.T. Sampath, S. Vukicevic, Characterization of receptors for osteogenic protein-1/bone morphogenetic protein-7 (OP-1/BMP-7) in rat kidneys, Kidney Int. 58 (2000) 1902–1911.
[38] T.D. Piscione, N.D. Rosenblum, The molecular control of renal branching morphogenesis: current knowledge and emerging insights, Differentiation 70 (2002) 227–246.
[39] S. Vukicevic, J.B. Kopp, F.P. Luyten, T.K. Sampath, Induction of nephrogenic mesenchyme by osteogenic protein 1 (bone morphogenetic protein 7), Proc. Natl. Acad. Sci. USA 93 (1996) 9021–9026.
[40] Y. Miyazaki, K. Oshima, A. Fogo, B.L. Hogan, I. Ichikawa, Bone morphogenetic protein 4 regulates the budding site and elongation of the mouse ureter, J. Clin. Invest. 105 (2000) 863–873.
[41] D.W. Lappin, R. McMahon, M. Murphy, H.R. Brady, Gremlin: an example of the re-emergence of developmental programmes in diabetic nephropathy, Nephrol. Dial. Transplant. 17 (Suppl. 9) (2002) 65–67.
[42] M. Zeichner-David, Is there more to enamel matrix proteins than biomineralization? Matrix Biol. 20 (2001) 307–316.
[43] T. Iwata, Y. Morotome, T. Tanabe, M. Fukae, I. Ishikawa, S. Oida, Noggin blocks osteoinductive activity of porcine enamel extracts, J. Dent. Res. 81 (2002) 387–391.
[44] V.A. Botchkarev, N.V. Botchkareva, M. Nakamura, O. Huber, K. Funa, R. Lauster, R. Paus, B.A. Gilchrest, Noggin is required for induction of the hair follicle growth phase in postnatal skin, FASEB J. 15 (2001) 2205–2214.
[45] V.A. Botchkarev, N.V. Botchkareva, A.A. Sharov, K. Funa, O. Huber, B.A. Gilchrest, Modulation of BMP signaling by noggin is required for induction of the secondary (nontylotrich) hair follicles, J. Invest. Dermatol. 118 (2002) 3–10.
[46] I. del Barco Barrantes, G. Davidson, H.J. Grone, H. Westphal, C. Niehrs, Dkk1 and noggin cooperate in mammalian head induction, Genes Dev. 17 (2003) 2239–2244.
[47] L. Grotewold, U. Ruther, The Wnt antagonist Dickkopf-1 is regulated by Bmp signaling and c-Jun and modulates programmed cell death, EMBO J. 21 (2002) 966–975.
[48] S. Piccolo, E. Agius, L. Leyns, S. Bhattacharyya, H. Grunz, T. Bouwmeester, E.M. De Robertis, The head inducer Cerberus is a multifunctional antagonist of Nodal, BMP and Wnt signals, Nature 397 (1999) 707–710.

Uterine sensitization-associated gene–1 (USAG-1), a novel BMP antagonist expressed in the kidney, accelerates tubular injury

Motoko Yanagita,[1] Tomohiko Okuda,[1] Shuichiro Endo,[2] Mari Tanaka,[2] Katsu Takahashi,[3] Fumihiro Sugiyama,[4] Satoshi Kunita,[4] Satoru Takahashi,[4] Atsushi Fukatsu,[5] Masashi Yanagisawa,[6,7] Toru Kita,[2] and Takeshi Sakurai[6,8]

[1]COE Formation for Genomic Analysis of Disease Model Animals with Multiple Genetic Alterations, [2]Department of Cardiovascular Medicine, and [3]Department of Oral and Maxillofacial Surgery, Graduate School of Medicine, Kyoto University, Kyoto, Japan. [4]Laboratory Animal Resource Center, Institute of Basic Medical Sciences, University of Tsukuba, Ibaraki, Japan. [5]Department of Artificial Kidneys, Graduate School of Medicine, Kyoto University, Kyoto, Japan. [6]Yanagisawa Orphan Receptor Project, Exploratory Research for Advanced Technology (ERATO), Japan Science and Technology Agency, Tokyo, Japan. [7]Howard Hughes Medical Institute and Department of Molecular Genetics, University of Texas Southwestern Medical Center, Dallas, Texas, USA. [8]Department of Pharmacology, Institute of Basic Medical Sciences, University of Tsukuba, Ibaraki, Japan.

Dialysis dependency is one of the leading causes of morbidity and mortality in the world, and once end-stage renal disease develops, it cannot be reversed by currently available therapy. Although administration of large doses of bone morphogenetic protein–7 (BMP-7) has been shown to repair established renal injury and improve renal function, the pathophysiological role of endogenous BMP-7 and regulatory mechanism of its activities remain elusive. Here we show that the product of *uterine sensitization-associated gene–1* (*USAG1*), a novel BMP antagonist abundantly expressed in the kidney, is the central negative regulator of BMP function in the kidney and that mice lacking USAG-1 (*USAG1*$^{-/-}$ mice) are resistant to renal injury. *USAG1*$^{-/-}$ mice exhibited prolonged survival and preserved renal function in acute and chronic renal injury models. Renal BMP signaling, assessed by phosphorylation of Smad proteins, was significantly enhanced in *USAG1*$^{-/-}$ mice with renal injury, indicating that the preservation of renal function is attributable to enhancement of endogenous BMP signaling. Furthermore, the administration of neutralizing antibody against BMP-7 abolished renoprotection in *USAG1*$^{-/-}$ mice, indicating that USAG-1 plays a critical role in the modulation of renoprotective action of BMP and that inhibition of USAG-1 is a promising means of development of novel treatment for renal diseases.

Introduction

Despite a significant increase in understanding of the pathophysiology of renal diseases, the incidence of end-stage renal disease (ESRD) is still increasing. Tubular damage and interstitial fibrosis are the final common pathway leading to ESRD (1, 2), irrespective of the nature of the initial renal injury, and the degree of tubular damage parallels the impairment of renal function (2). Once tubular damage is established, it cannot be reversed or repaired by currently available treatment, and renal function deteriorates to renal failure, which is often life threatening (3). If we can come up with an agent that can reverse established tubular damage, it would significantly reduce the need for dialysis. Bone morphogenetic protein–7 (BMP-7) is a promising candidate for such an agent, because it is reported to protect the kidney from renal injury (4–8). BMP-7 is known to play essential roles in kidney development, because BMP-7–null mice die shortly after birth due to severe renal hypoplasia (9, 10). BMP-7 is also abundant in the adult kidney, especially in distal tubule epithelial cells (11, 12). Recently, several reports indicated that the expression of BMP-7 is decreased in renal disease models (5, 6, 13–16) and that administration of recombinant BMP-7 at pharmacological doses repairs chronic renal injury (4–8). However, the pathophysiological role and regulatory mechanism of endogenous BMP-7 remain elusive.

The local activity of endogenous BMP is controlled not only by regulation of its expression, but also by certain classes of molecules termed BMP antagonists (17). BMP antagonists function through direct association with BMP, thus inhibiting the binding of BMP to its receptors. *Uterine sensitization-associated gene–1* (*USAG1*) encodes a secreted protein and was initially found as a gene of unknown function whose expression was upregulated in sensitized endometrium of the rat uterus (18). Recently, Avsian-Kretchmer et al. suggested USAG-1 as a candidate for a novel BMP antagonist using bioinformatic analysis (19). Furthermore, Laurikkala et al. demonstrated USAG-1 to be a BMP antagonist expressed in teeth (20).

We independently identified USAG-1 to be a novel BMP antagonist, abundantly expressed in the kidney (21). The expression of USAG-1 is abundant in renal tubules and teeth in late embryogenesis and in adult tissues it is by far most abundant in the kidney, especially in the distal tubule with a pattern similar to that of BMP-7. From these findings, we hypothesized that USAG-1 might regulate the renoprotective action of BMP-7 in the adult kidney.

To evaluate this hypothesis, we generated *USAG1*-knockout (*USAG1*$^{-/-}$) mice and induced acute and chronic renal disease models in which renal tubules, but not glomeruli, were mainly damaged.

Nonstandard abbreviations used: BMP-7, bone morphogenetic protein-7; EMT, epithelial-mesenchymal transition; MCP-1, monocyte chemotactic protein-1; PTEC, proximal tubule epithelial cell; USAG1, uterine sensitization-associated gene-1; UUO, unilateral ureteral obstruction.

Conflict of interest: The authors have declared that no conflict of interest exists.

Citation for this article: *J. Clin. Invest.* **116**:70–79 (2006). doi:10.1172/JCI25445.

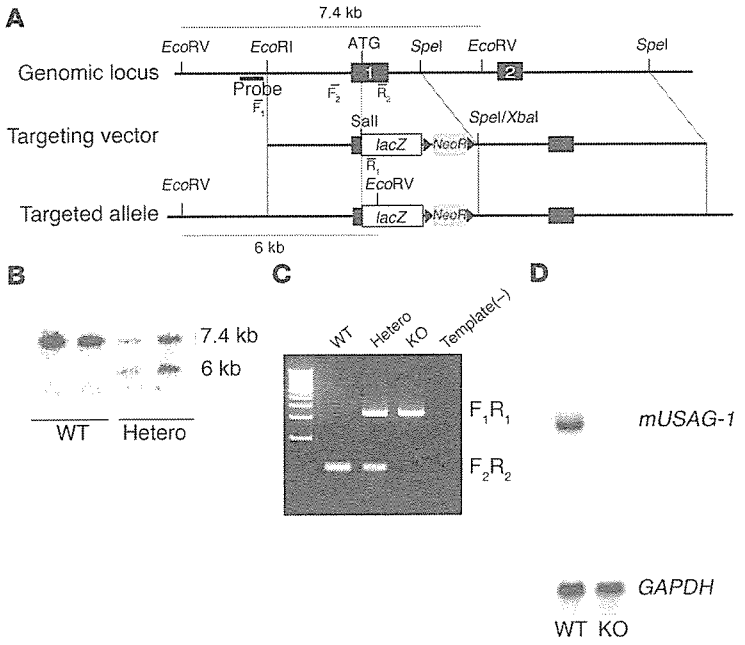

Figure 1
Generation of *USAG1*$^{-/-}$ mutation by gene targeting. (**A**) *USAG1*–null allele was generated by homologous recombination in ES cells. Exon 1 (black box) and part of the intron were replaced with a *lacZ* gene (white box) and the *Neo*R cassette (gray box). (**B**) Analysis of *USAG1*$^{+/+}$ (WT) and correctly targeted heterozygous (Hetero) ES cell clones by Southern blot analysis using 5′ genomic probe (thick black line in **A**). (**C**) PCR genotyping of F_2 littermates. Template(–) is the negative control. (**D**) Northern blot analysis of *USAG1* mRNA in the kidney of *USAG1*$^{+/+}$ and *USAG1*$^{-/-}$ (KO) mice.

Results

Generation and analysis of USAG1$^{-/-}$ *mice.* *USAG1*$^{-/-}$ mice were generated by deleting the first exon including the transcription initiation codon, the signal peptide, and the following 46 amino acids (Figure 1). *USAG1*$^{-/-}$ mice were born at the ratio expected according to Mendel's law of heredity and were viable, fertile, and appeared healthy except that they exhibited supernumerary teeth, both in the incisors and molars, and fused teeth in the molar region (Supplemental Figure 1; supplemental material available online with this article; doi:10.1172/JCI25445DS1). Although there was variation in the sites of extra teeth and fused teeth, this tooth phenotype was fully penetrant. Food consumption was not disturbed by this tooth phenotype in *USAG1*$^{-/-}$ mice (data not shown).

Attenuated acute tubular injury in USAG1$^{-/-}$ *mice.* To induce acute tubular injury, we utilized a cisplatin nephrotoxicity model (22–24). Administration of a nephrotoxic agent, cisplatin, to wild-type littermates caused acute tubular injury that resulted in severe renal failure. Within the first 3 days, 54% of wild-type mice died, while 92% of *USAG1*$^{-/-}$ mice survived the period (Figure 2A). The renal function of *USAG1*$^{-/-}$ mice on day 3 was significantly preserved compared with that in wild-type littermates (Figure 2B). Histological examination of the kidneys of wild-type mice on day 3 showed severe proximal tubular damage, while this change was markedly reduced in *USAG1*$^{-/-}$ mice (Figure 2, C and D). Expression of E-cadherin, a marker for tubular epithelial integrity (25), was markedly reduced in the kidneys of wild-type mice, while its expression was preserved in *USAG1*$^{-/-}$ mice (Figure 2E). Tubular apoptosis, a characteristic feature of tubular injury in cisplatin nephrotoxicity (23), was also significantly reduced in *USAG1*$^{-/-}$ mice (Figure 2F). As reported previously (24), cisplatin administration resulted in upregulation of TNF-α, IL-1β, monocyte chemotactic protein-1 (MCP-1), TGF-β1, and type IV collagen expression in the kidney of wild-type mice. However, the induction of these genes was completely abolished in *USAG1*$^{-/-}$ mice (Figure 2G). Infiltration of macrophages and monocytes in the kidney was also significantly reduced in *USAG1*$^{-/-}$ mice (Figure 2H), in accordance with the reduction of MCP-1 expression (Figure 2G). Expression of BMP-7 was comparable between wild-type mice and *USAG1*$^{-/-}$ mice before and after injection of cisplatin (Figure 2G).

Renal fibrosis is reduced in USAG1$^{-/-}$ *mice.* As a model of chronic renal injury, we performed unilateral ureteral obstruction (UUO) (26, 27) in both *USAG1*$^{-/-}$ mice and wild-type mice, and the kidneys were harvested 14 days after the operation. In wild-type mice, the obstructed kidney showed dilatation/degeneration of renal tubules and interstitial fibrosis, whereas the normal architecture was preserved in *USAG1*$^{-/-}$ mice, except for mild dilatation of tubules (Figure 3, A and B). Expression of E-cadherin was markedly reduced in the kidneys of wild-type mice, while its expression was preserved in *USAG1*$^{-/-}$ mice (Figure 3C). Furthermore, expression of α-SMA, a marker of tubulointerstitial myofibroblasts (28), was upregulated in the interstitium of the obstructed kidney of wild-type mice, while high expression of α-SMA was restricted to vascular smooth muscle cells in *USAG1*$^{-/-}$ mice (Figure 3D). Since expansion and fibrosis of the renal interstitium is another characteristic feature of UUO (6), we examined the deposition of type IV collagen, which is a normal component of the tubular basement membrane. The basement membranes of neighboring tubules are adjacent to each other in the normal kidney. In the obstructed kidney of wild-type mice, expansion of the interstitial component increased the distance between adjacent basement membranes, and type IV collagen produced by interstitial myofibroblasts was aberrantly expressed in the interstitium. However, in the obstructed kidney of *USAG1*$^{-/-}$ mice, the distance between the basement membranes was significantly smaller than that in wild-type mice (Figure 3E). Expression of TNF-α, IL-1β, MCP-1, TGF-β1, and type IV collagen was markedly upregulated on day 14 in the obstructed kidney of wild-type mice. In contrast, the induction of these genes was significantly attenuated, by 33%, 46%, 37%, 75%, and 23%, respectively, in *USAG1*$^{-/-}$ mice (Figure 3F). Expression of BMP-7 in the obstructed kidney was comparable in wild-type mice and *USAG1*$^{-/-}$ mice.

BMP signaling is enhanced in USAG1$^{-/-}$ *mice.* To evaluate whether the reduction in renal injury in *USAG1*$^{-/-}$ mice is attributable to enhanced BMP signaling, phosphorylation of Smad1/5/8 in the kidney was examined in both models (Figure 4). After the induction of kidney disease models, phosphorylation of Smad1/5/8 was hardly detected in wild-type mice, while in *USAG1*$^{-/-}$mice, the phosphorylation was preserved in the nuclei of tubular epithelial cells (Figure 4A). To examine the specificity of the antibody against phospho-Smad1/5/8, we performed double immunostaining using anti-phospho-Smad1/5/8 antibody and anti-phospho-Smad2/3, and found that most of the nuclei positive for phospho-Smad1/5/8 were negative for phospho-Smad2/3 (Figure 4B), indicating the

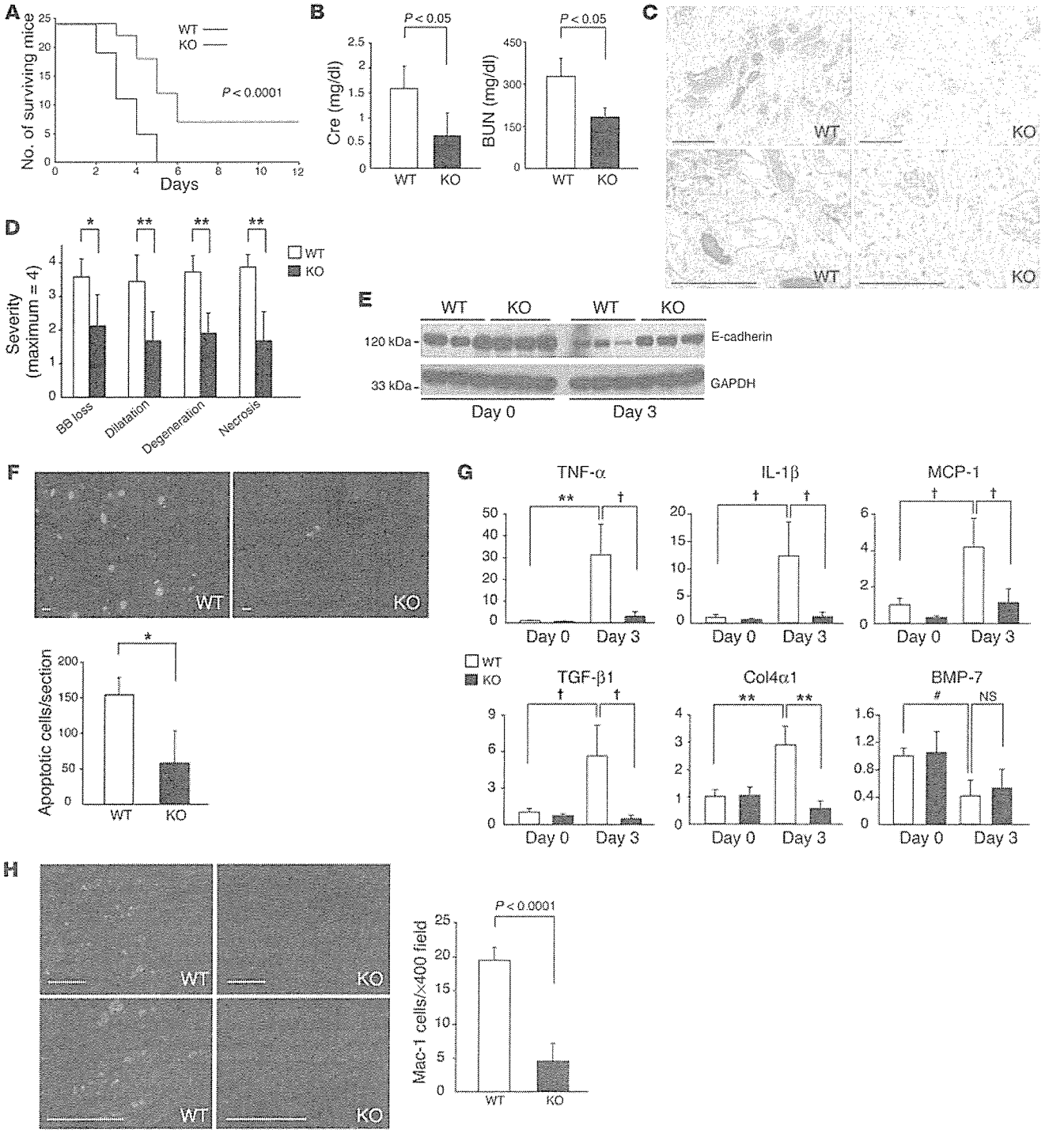

Figure 2

USAG1$^{-/-}$ mice showed less renal injury in cisplatin nephrotoxicity. (**A**) Survival curves of wild-type mice (black line) and *USAG1*$^{-/-}$ mice (red line) after cisplatin administration ($n = 24$). (**B**) Serum creatinine (Cre) and blood urea nitrogen (BUN) levels at 3 days after injection of cisplatin ($n = 6$). (**C**) Representative renal histological findings in wild-type mice and *USAG1*$^{-/-}$ mice on day 3. Scale bars: 100 μm. (**D**) Semiquantitative evaluation of morphologic kidney damage, expressed as relative severity on a scale from 0 to 4 ($n = 6$). Morphological findings were scored according to proximal tubule brush border loss (BB loss), tubule dilatation (Dilatation), tubule degeneration (Degeneration), and tubule necrosis (Necrosis). $^{*}P < 0.01$; $^{**}P < 0.001$. (**E**) E-cadherin expression in cisplatin nephrotoxicity. Kidney lysates were subjected to immunoblotting with anti–E-cadherin antibody. Representative data from 4 independent experiments are shown. (**F**) TUNEL staining of kidneys on day 3 of cisplatin nephrotoxicity. The number of TUNEL-positive cells per section was counted in transverse sections ($n = 6$). Scale bars: 10 μm. (**G**) Gene expression in cisplatin nephrotoxicity. Gene expression was determined by real-time RT-PCR. In each experiment, expression levels were normalized to the expression of GAPDH and expressed relative to mice on day 0. $n = 4$–6 for each experiment. $^{\dagger}P < 0.005$; $^{\#}P < 0.02$. Col4α1, collagen type IV α 1. (**H**) Infiltration of Mac-1–positive cells after cisplatin injection. The number of Mac-1–positive cells per field was counted in 10 consecutive fields ($n = 6$). Scale bars: 100 μm.

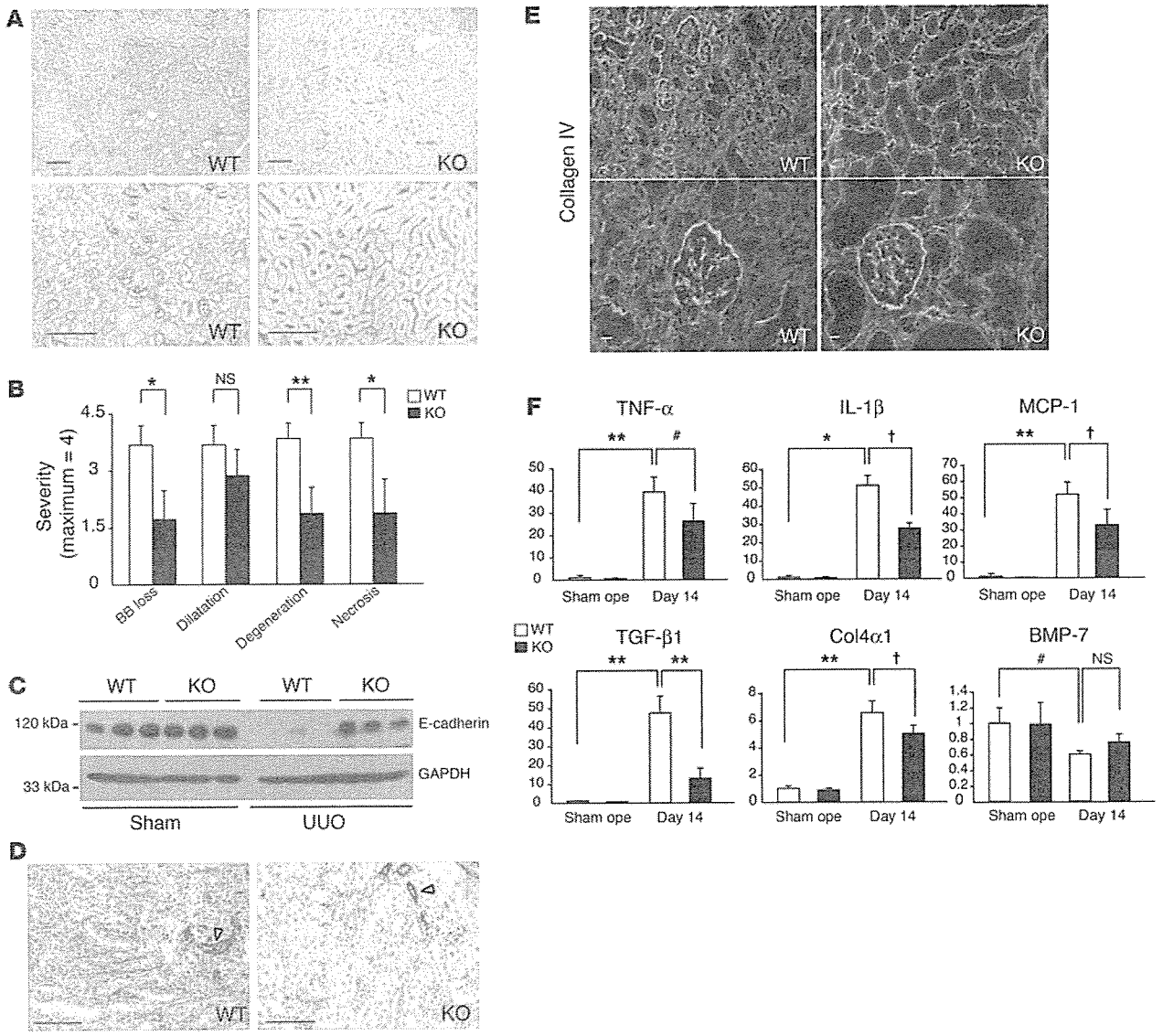

Figure 3

USAG1$^{-/-}$ mice showed reduced EMT and tubulointerstitial fibrosis in UUO. (**A**) Representative histology of the obstructed kidney in wild-type mice and *USAG1*$^{-/-}$ mice 14 days after the operation. Scale bars: 100 μm. (**B**) Semiquantitative evaluation of morphologic kidney damage in wild-type mice and *USAG1*$^{-/-}$ mice, expressed as relative severity on a scale from 0 to 4 ($n = 6$). (**C**) E-cadherin expression in UUO. Kidney lysates were subjected to immunoblotting with anti–E-cadherin antibody. Representative data from 4 independent experiments are shown. (**D**) Immunostaining of α-SMA in UUO. Arrowheads indicate vascular smooth muscle cells. (**E**) Immunostaining of type IV collagen in UUO. Scale bars: 10 μm. (**F**) Gene expression in UUO. Gene expression was determined by real-time RT-PCR. In each experiment, the expression levels were normalized to the expression of GAPDH and expressed relative to expression in mice on day 0. $n = 4$–6 for each experiment. $^{\#}P < 0.01$; $^{\dagger}P < 0.005$; $^{*}P < 0.001$; $^{**}P < 0.0001$. Sham ope, mice 14 days after sham operation; day 14, mice 14 days after UUO.

specificity of the antibody against phospho-Smad1/5/8. We also examined the phosphorylation of Smad1/5/8 in immunoblotting of kidney lysates and demonstrated that the phosphorylation was preserved in the kidneys of *USAG1*$^{-/-}$ mice, while it was downregulated in WT mice (Figure 4C). No difference was observed in the phosphorylation of Smad1/5/8 prior to disease induction between *USAG1*$^{-/-}$ mice and WT mice (Figure 4, A and C).

Blocking BMP-7 activity abolishes renoprotection in USAG1$^{-/-}$*mice.* To analyze the mechanism of renoprotection in *USAG1*$^{-/-}$mice, we administered a neutralizing antibody against BMP-7 to *USAG1*$^{-/-}$ mice in both kidney disease models. First we evaluated the specificity of the neutralizing activity of the antibody using an assay measuring alkaline phosphatase activity and phosphorylation of Smad1/5/8 in C2C12 cells induced by BMPs. Addition of the antibody inhibited the alkaline phosphatase activity and phosphorylation of Smad1/5/8 induced by BMP-7, but not by BMP-4 (Figure 5A) or BMP-2 (data not shown), indicating the specificity of the antibody. As a negative control, we used isotype-matched IgG2B. Next we administered a neutralizing antibody against BMP-7 to *USAG1*$^{-/-}$ mice with cisplatin nephrotoxicity. Of 7 mice treated with neutralizing antibody, 2 mice died on day 2 and 1 mouse died on day 3, while none of the mice treated with isotype-matched IgG2B

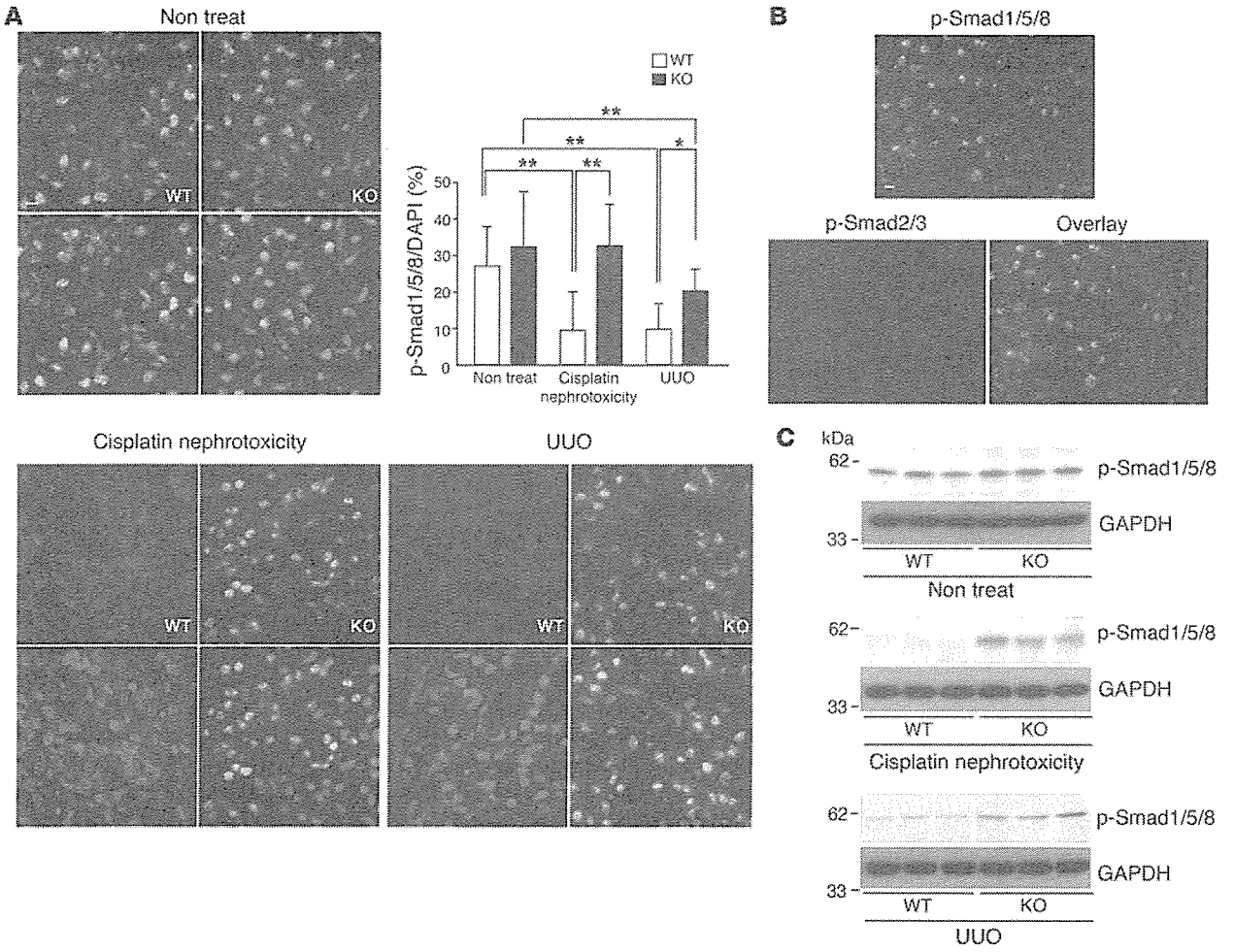

Figure 4
Enhanced BMP signaling in kidneys of *USAG1*$^{-/-}$ mice. (**A**) Phosphorylation of Smad1/5/8 in kidneys of *USAG1*$^{-/-}$ mice and WT mice. The number of pSmad1/5/8-positive nuclei (upper panels) was counted in 10 consecutive fields in each specimen and normalized by the number of DAPI-positive nuclei (lower panels). $n = 6$. Scale bar: 10 μm. $^{*}P < 0.001$; $^{**}P < 0.0001$. Non treat, mice without disease models. (**B**) Double immunostaining of phospho-Smad1/5/8 and phospho-Smad2/3. Almost all the nuclei positive for pSmad1/5/8 were negative for pSmad2/3. Scale bar: 10 μm. (**C**) Immunoblotting of phospho-Smad1/5/8 in kidney lysates prior to disease induction and in both kidney disease models. Representative data from 5 independent experiments are shown.

died within the first 3 days. Administration of neutralizing antibody also resulted in a deterioration of renal function measured by elevation of serum creatinine to a level similar to that in WT mice, while administration of IgG2B did not (Figure 5B). Furthermore, histological examination of the kidneys of *USAG1*$^{-/-}$ mice treated with neutralizing antibody demonstrated severely damaged proximal tubular epithelial cells, while these changes were absent in mice treated with IgG2B (Figure 5B). We also administered the neutralizing antibody to *USAG1*$^{-/-}$ mice with UUO and found that type IV collagen expression in the obstructed kidney was increased in *USAG1*$^{-/-}$ mice treated with neutralizing antibody, but not in those administered IgG2B (Figure 5C). Histological examination of the obstructed kidneys of *USAG1*$^{-/-}$ mice treated with neutralizing antibody demonstrated severe interstitial fibrosis, while this change was almost absent in mice treated with IgG2B (Figure 5C).

USAG1 is the most abundant BMP antagonist in adult kidney. Finally we analyzed the expression of USAG-1 and other BMP antagonists in adult kidneys using modified real-time PCR and in situ hybridization (Figure 6). To compare the expression levels of different genes in real-time PCR, we set the standard curve with the plasmid encoding each BMP antagonist at various concentrations and analyzed the copy number of each gene contained in kidney cDNA. Among known BMP antagonists, USAG-1 was by far the most abundant in the kidneys, and twisted gastrulation was the second most abundant BMP antagonist. We also analyzed the localization of BMP antagonists in the kidneys using in situ hybridization and found that the expression of USAG-1 was confined to distal tubules, as previously described (21), with a pattern similar to that of BMP-7 (12). Expression of twisted gastrulation was also detected in some distal tubules; however, the intensity of the signal was much lower than that of USAG-1, in accordance with the results of real-time PCR. Differential screening–selected gene aberrative in neuroblastoma (DAN) and protein related to DAN and Cerberus (PDRC) were faintly observed in the inner medulla, and other BMP antagonists were not detected with this method.

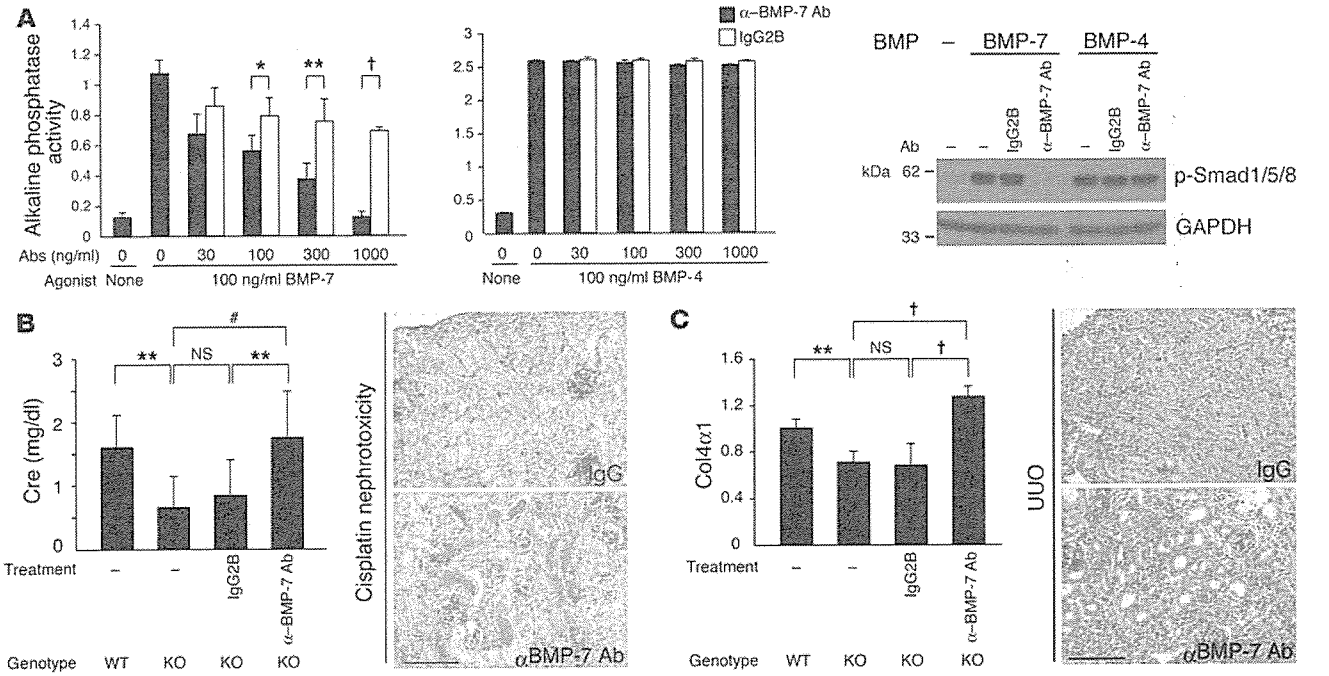

Figure 5

Blocking BMP-7 activity abolishes renoprotection in *USAG1*$^{-/-}$ mice. (**A**) Evaluation of neutralizing activity of anti–BMP-7 antibody. Anti–BMP-7 antibody inhibits alkaline phosphatase activity and phosphorylation of Smad1/5/8 induced by BMP-7, but not by BMP-4. (**B**) Serum creatinine level of *USAG1*$^{-/-}$ mice treated with anti–BMP-7 antibody and representative histological findings on day 3 of cisplatin nephrotoxicity. Scale bar: 100 μm. (**C**) Gene expression of type IV collagen in kidneys of *USAG1*$^{-/-}$ mice treated with anti–BMP-7 antibody and representative histological findings on day 14 of UUO. $^{*}P < 0.1$; $^{**}P < 0.01$; $^{\#}P < 0.001$; $^{\dagger}P < 0.0001$.

Discussion

Epithelial-mesenchymal transition (EMT) is a necessary step for renal fibrosis, as well as in embryonic development and tumor progression (29–31). TGF-β is known to stimulate EMT, while BMP-7 inhibits and reverses the transition (3). Zeisberg et al. recently reported that BMP-7 reverses TGF-β1–induced EMT and induces mesenchymal-epithelial transition in vitro (4, 32). They further demonstrated that administration of a pharmacological dose of BMP-7 resulted in regression of established lesions in the kidney and improved renal function. In this report, we demonstrated that deficiency of USAG-1, a novel BMP antagonist in the kidney, results in marked preservation of renal function by reinforcement of BMP signaling.

Based on these findings, we set the working hypothesis: in many types of renal disease, proximal tubule epithelial cells (PTECs) are the main site of injury (33) and undergo EMT, which causes loss of structural integrity of epithelial cells characterized by a reduction of E-cadherin expression and the induction of α-SMA in interstitial myofibroblasts (Figure 7A). BMP-7 secreted from distal tubules (12) inhibits EMT of PTECs and induces redifferentiation of mesenchymal cells to epithelial cells. USAG-1 produced from distal tubules binds to BMP-7 and inhibits its renoprotective action by interfering with binding to its receptors.

In addition to the inhibition of EMT, many other pharmacological actions of BMP-7 have been reported. Administration of recombinant BMP-7 inhibits the induction of inflammatory cytokine expression in the kidney (12), attenuates inflammatory cell infiltration (6), and reduces apoptosis of tubular epithelial cells in renal disease models (34) (Figure 7A). These phenomena are also observed in *USAG1*$^{-/-}$ mice, and the similarity between BMP-7–treated animals and *USAG1*$^{-/-}$ mice strongly supports our working model that deficiency of USAG-1 reinforces the renoprotective activities of BMP.

In accordance with this hypothesis, the renoprotection in *USAG1*$^{-/-}$ mice was abolished in both renal disease models when a neutralizing antibody against BMP-7 was administered (Figure 5). These results strongly support the hypothesis, and BMP-7 is a potent candidate for the counterpart of USAG-1.

We also observed preserved phosphorylation of Smad1/5/8 in the kidneys of *USAG1*$^{-/-}$ mice in both renal disease models, suggesting that BMP signaling was enhanced in *USAG1*$^{-/-}$ mice, while no difference was observed between WT and KO mice in phosphorylation of Smad1/5/8 prior to disease induction (Figure 4, A and C). We assume that BMP signaling prior to disease induction might be potent enough to cause full phosphorylation of Smad1/5/8 regardless of the presence or absence of USAG-1, while in the later stages of kidney diseases, BMP signaling is decreased and the presence of USAG-1 might cause a further reduction in BMP signaling.

Furthermore, we demonstrated that USAG-1 is by far the most abundant BMP antagonist in the kidney (Figure 6A). Because other BMP antagonists also antagonize BMP-7 activities (Supplemental Figure 2), we conclude that USAG-1 plays an important role in the modulation of BMP activities in the kidney not because of its ligand specificity, but because of its high expression among other BMP antagonists. In addition, the tissue localization of USAG-1 (Figure 6B) is quite similar to that of BMP-7 (12), and USAG-1 can effectively access and inactivate BMP-7 at the site of production.

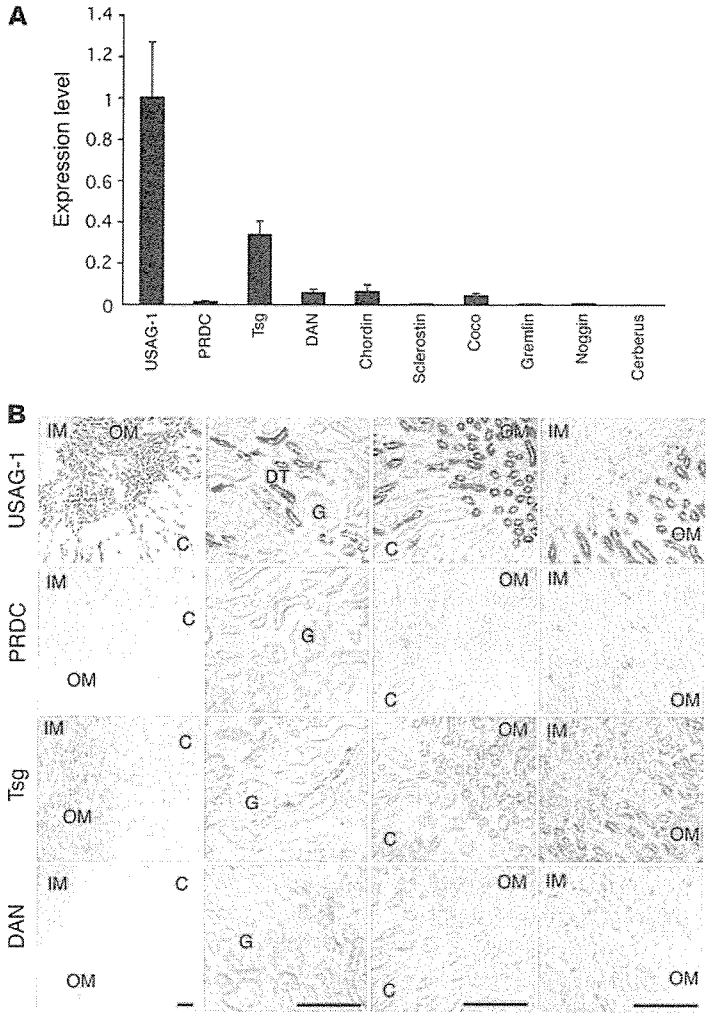

Figure 6
Expression of BMP antagonists in kidney. (**A**) Kidney cDNA of wild-type mice with Svj background was subjected to real-time PCR with various primers for BMP antagonists, and the standard curve was set using the plasmid encoding each BMP antagonist from concentrations of 1 pg/μl to 1 fg/μl. The values of each BMP antagonist in the kidney cDNA were multiplied by the length of the vectors and normalized to the value of USAG-1 expression (n = 4–5). Expression of USAG-1 was by far the most abundant in the kidney among other BMP antagonists. Tsg, twisted gastrulation. (**B**) Kidney sections were subjected to in situ hybridization with probes for all BMP antagonists. Expression of USAG-1 was confined to the distal tubular epithelial cells. Twisted gastrulation was also sparsely expressed in some distal tubules. Differential screening–selected gene aberrative in neuroblastoma (DAN) and protein related to DAN and Cerberus (PDRC) were faintly detected in the inner medulla. Expression of other BMP antagonists was not detected by this method. Scale bars: 100 μm. IM, inner medulla; OM, outer medulla; C, cortex; DT, distal tubule; G, glomerulus.

Although we illustrated USAG-1/BMP-7 binding as occurring outside of PTECs in Figure 7A, it might be possible that the binding occurs intracellularly within the secretory pathway in PTECs and that USAG-1 and BMP-7 are secreted in complex form. Further investigations are necessary to clarify this point.

Interestingly, the expression of USAG-1 decreased during the course of disease models (Supplemental Figure 3 and unpublished observations). We assume that the reduction of USAG-1 in renal diseases is a self-defense mechanism to minimize its inhibitory effect on BMP signaling. Because the reduction in USAG-1 expression in WT mice is not enough to overcome the reduction in BMP-7 expression, further reduction or abolishment of the action of USAG-1 is desirable for the preservation of renal function, and the results of the present study justify therapy targeted toward USAG-1. For example, drugs or neutralizing antibodies that inhibit binding between USAG-1 and BMP or gene-silencing therapy for *USAG1* would enhance the activity of endogenous BMP and might be a promising way to develop novel therapeutic methods for severe renal disease (Figure 7B). Because the expression of USAG-1 is confined to the kidney in adult mice and humans (21), it would be a better target for kidney-specific therapeutic trials. On the other hand, administration of recombinant BMP-7, whose target cells are widely distributed throughout the body, might produce some additional extrarenal actions, including beneficial effects, such as actions on renal osteodystrophy (35–39) and vascular calcification (40, 41).

Furthermore, these therapies targeted toward USAG-1 might protect the kidney during administration of nephrotoxic agents such as cisplatin. The pathological roles of USAG-1 in glomerular injury should be further elucidated before we undertake therapeutic trials against USAG-1.

Despite the essential role of BMP-7 in renal development, we did not observe any developmental abnormality in the kidney of *USAG1*$^{-/-}$ mice with this genetic background. We assume that there are many reasons for the lack of developmental abnormality: First, USAG-1 expression in the developing kidney is not apparent on embryonic day 11.5 (21), whereas BMP-7 expression is intense in the metanephric mesenchyme (42) with a pattern similar to that of gremlin (43). In the later stages, USAG-1 expression appears in the tubular epithelium in the medullary region (21), whereas BMP-7 expression is confined to the condensed mesenchyme and peripheral ureteric epithelium (42). Therefore, the expression pattern of USAG-1 in the developing kidney is totally different from that of BMP-7. Second, the expression of USAG-1 is very low in early embryogenesis, increases toward the late stage of embryogenesis, and is much higher in the adult kidney (21), while the expression of gremlin is high in early embryogenesis with a pattern similar to that of BMP-7, and becomes almost undetectable in the healthy adult kidney (Figure 6). Furthermore, *gremlin*-deficient mice show severe developmental abnormality in the kidney, which is quite similar to that of *BMP-7*-deficient mice. Therefore, we conclude that gremlin is a regulator of BMP-7 activity in the developing kidney, and lack of USAG-1 might be compensated by gremlin and does not cause any developmental abnormality in the kidney.

Recently another function of USAG-1 as a modulator of Wnt signaling has been reported in *Xenopus* embryogenesis (44). Although the role of the Wnt pathway in the progression of renal diseases remains to be elucidated, there is a possibility that modulation of the Wnt pathway might also play some roles in the preservation of renal function in *USAG1*$^{-/-}$ mice. Close relationships between the Wnt and BMP pathways have also been reported; for instance, dickkopf homolog 1 (DKK1), a Wnt antagonist, and noggin, a BMP antagonist, cooperate in head induction, while the expression of

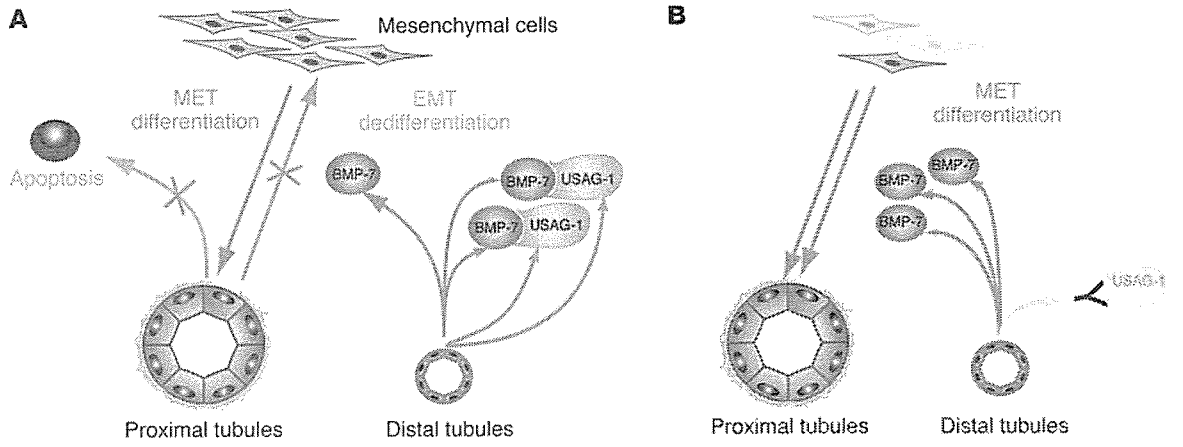

Figure 7
Working model of role of BMP-7 and USAG-1 in renal diseases. (**A**) In renal injury, PTECs are mainly damaged and undergo EMT to fibroblast-like mesenchymal cells. BMP-7 secreted by the distal tubule inhibits EMT and apoptosis of PTECs. USAG-1 is also secreted by the distal tubule, binds to BMP-7, and inhibits the renoprotective actions of BMP-7. (**B**) Therapeutic implication of USAG-1. Reduction of USAG-1 activity, for example, by a neutralizing antibody blocking the binding of USAG-1 and BMP-7, results in reinforcement of the renoprotective action of BMP-7. MET, mesenchymal-epithelial transition.

DKK1 is regulated by BMP-4 in limb development. Furthermore, a BMP antagonist, cerberus, has binding sites for both Wnt and BMP and antagonizes the activities of both the Wnt and BMP signaling pathways. USAG-1 might also have dual activities and act as a molecular link between these 2 important signaling pathways.

In conclusion, this study showed that USAG-1 plays important roles in the progression of renal diseases and might be a potent negative regulator of the renoprotective action of endogenous BMP signaling. Recently, Lin et al. identified a positive regulator of BMP-7 named kielin/chordin-like protein (KCP) and demonstrated that *KCP*$^{-/-}$ mice are susceptible to tubular injury and interstitial fibrosis (45). These data support the idea that BMP-7 protects the kidney from renal injury. Because these negative and positive modulators of BMP signaling regulate and edge the boundaries of BMP activity, further understanding of these modulators would give valuable information about their pathophysiological functions and provide a rationale for a therapeutic approach against these proteins.

Methods

Generation of USAG1$^{-/-}$ *mice.* We isolated a genomic fragment containing the mouse *USAG1* gene by screening a 129/SvJ genomic library (Stratagene). We inserted an *nlacZ* gene and a PGK-*Neo*R cassette in the opposite transcriptional orientation to the *USAG1* gene. ES cells were transfected with the linearized targeting vector by electroporation and selected by G418-containing medium. Homologous recombinants were screened and identified by genomic Southern blot analysis with an *Hin*cII-*Eco*RI probe mapping outside the 5′ homology arm (Figure 1A). Homologous recombined ES cell clones were obtained, and correct recombination was confirmed by Southern blot (Figure 1B) as well as PCR analyses. ES cells carrying the *USAG1*-null allele were injected into C57BL/6 blastocysts to obtain chimeric mice, which were crossed with wild-type C57BL/6J mice. Following germline transmission, the mice were maintained in a mixed SvJ background. PCR genotyping was used for all subsequent studies to allow specific detection of both the wild-type and *USAG1*$^{-/-}$ alleles (Figure 1C). Sequences of the primers used for genotyping are as follows: F1, CCCCTCCTCATCTGGCTGCTTCCTAAACGG; R1, CAGTCACGACGTTGTAAAACGACGGGATCC; F2, GGGATCCCACCCCTTCTCT; and R2, GCCGGGACAGGTTTAACCA.

Animal use. All experiments except those represented in Supplemental Figure 3 were performed using *USAG1*$^{-/-}$ mice and their wild-type littermates (*USAG1*$^{+/+}$) of the F_2 generation. All mice were housed in specific pathogen-

Table 1
Primers for real-time RT-PCR

Gene	Sequence of primers (5′-3′)
GAPDH	CCAGAACATCATCCCTGCATC; CCTGCTTCACCACCTTCTTGA
TNFα	ATGAGAAGTTCCCAAATGGCC; CCTCCACTTGGTGGTTTGCTA
IL-1β	CCTTCCAGGATGAGGACATGA; AACGTCACACACCAGCAGGTT
TGFβ1	GCAACAATTCCTGGCGTTACC; CGAAAGCCCTGTATTCCGTCT
MCP-1	TGCATCTGCCCTAAGGTCTTC; AAGTGCTTGAGGTGGTTGTGG
Col4α1	TTCCTTCGTGATGCACACCA; TTCTCATGCACACTTGGCAGC
USAG1	GCAACAGCACCCTGAATCAAG; TGTATTTGGTGGACCGCAGTT
Chordin	GCAGTGGTTCCCAGAGAATCA; AACAATCGTCCCGCTCACAGT
DAN	CTTCAGTTACAGCGTCCCCAA; CCAAGGTCACAATCTCCCACA
PRDC	AGGAGGCTTCCATCTCGTCAT; CCGGTTCTTCCGTGTTTCA
Twisted gastrulation	AAACGTGTCTGTTCCCAGCAA; ACACTGGTGGATGGACATGCA
Gremlin	AGCCCAAGAAGTTCACCACCA; TATGCAACGGCACTGCTTCAC
Sclerostin	CAAGCCTTCAGGAATGATGCC; TCGGACACATCTTTGGCGT
Noggin	AGAAACAGCGCCTGAGCAAGA; AAAAGCGGCTGCCTAGGTCAT
Cerberus	CCCATCAAAAGCCACGAAGT; CCAAAGCAAAGGTTGTTCTGG
Coco	TCCGCTTTTAGCCACTAGGTG; GCTGTTATTCTGGTGTCCCCA
BMP-2	TCGACCATGGTGGCCGGGACCCG; TGTTCCCGGAAGATCTGGAGT
BMP-3	AGCGAATGGATTATCTCTCCCA; TCTTTTCCGGCACACAGCA
BMP-4	CTGGAATGATTGGATTGTGGC; GCATGGTTGGTTGAGTTGAGG
BMP-5	AAGCCTGCAAGAAGCACGAA; GGAAAAGAACATTCCCCGTCA
BMP-6	CCAACCACGCCATTGTACAGA; GGAATCCAAGGCAGAACCATG
BMP-7	TGTGGCAGAAAACAGCAGCA; TCAGGTGCAATGATCCAGTCC

free conditions. Experiments represented in Supplemental Figure 3 were performed using C57BL/6 mice. All animal experiments were approved by the Animal Research Committee at the Graduate School of Medicine, Kyoto University, and the Animal Experiment and Use Committee at the University of Tsukuba and were in accordance with NIH guidelines.

Cisplatin administration. Cisplatin (Sigma-Aldrich) was administered at 20 mg/kg to mice by a single intraperitoneal injection. Mice were sacrificed 72 hours after administration of cisplatin, and tissue and blood were collected for further analysis.

UUO. Complete UUO was performed as previously described (46). Briefly, under sodium pentobarbital anesthesia, the middle portion of the left ureter was ligated and cut between 2 ligated points. At 14 days after surgery, the mice were sacrificed, and the obstructed kidneys were subjected to the studies described below.

Histological studies. The kidneys were fixed in Carnoy solution and embedded in paraffin. Sections (2 μm) were stained with PAS for routine histological examination, and the degree of morphological changes was determined using light microscopy. The following parameters were chosen as indicative of morphological damage to the kidney after cisplatin injection and UUO: brush border loss, tubule dilatation, tubule degeneration, and tubule necrosis. These parameters were evaluated on a scale of 0 to 4, and classed as: 0, not present; 1, mild; 2, moderate; 3, severe; and 4, very severe. The remaining kidney was used for immunohistochemical study, RNA isolation, and protein extraction.

Immunostaining. Frozen sections of kidneys were subjected to immunostaining with polyclonal antibodies against type IV collagen (ICN Pharmaceuticals), phosphorylated Smad1/5/8 (Cell Signaling Technology), and phosphorylated Smad2/3 (Santa Cruz Biotechnology Inc.) and monoclonal antibodies against α-SMA (Sigma-Aldrich) and Mac-1 (BD Biosciences – Pharmingen) as previously described (47, 48).

Immunoblotting. Whole kidney protein was homogenized in RIPA buffer (50 mM Tris at pH 7.5, 150 mM NaCl, 1% Nonidet P-40, 0.25% SDS, 1 mM Na_3VO_4, 2 mM EDTA, 1 mM PMSF, and 10 μg/ml aprotinin) and subjected to immunoblotting as described previously (49). Anti-E-cadherin antibody and anti-GAPDH antibody were from BD Biosciences – Transduction Laboratories and Research Diagnostic Inc., respectively.

Apoptosis detection and quantification. The TUNEL technique (In Situ Cell Death Detection Kit; Roche Diagnostics GmbH) was used to detect apoptotic cells in situ. All apoptotic nuclei within a transverse section at the renal pelvis were counted.

Quantification of mRNA by real-time RT-PCR. Real-time RT-PCR was performed with a 7700 Sequence Detection System (Applied Biosystems). Five micrograms of total RNA was reverse transcribed in a reaction volume of 20 μl using Superscript III reverse transcriptase and random primers (Invitrogen Corp.). The product was diluted to a volume of 400 μl, and 5-μl aliquots were used as templates for amplification using SYBR Green PCR amplification reagent (Applied Biosystems) and gene-specific primers. Specific primers for each gene transcript (listed in Table 1) were designed using Primer Express software version 2.0.0 (Applied Biosystems) and checked as to whether they showed a single peak in the dissociation curve. Serially diluted cDNA or plasmids encoding probes for in situ hybridization were used to generate the standard curve for each primer, and the PCR conditions were as follows: 50°C for 2 minutes, 95°C for 10 minutes, then 95°C for 15 seconds and 60°C for 1 minute for 40 cycles.

Administration of neutralizing antibody against BMP-7. In cisplatin nephrotoxicity, 1.5 mg/kg neutralizing anti-BMP-7 antibody (R&D Systems Inc.) was peritoneally injected into *USAG1*$^{-/-}$ mice 24 hours after injection of cisplatin. In UUO, 0.5 mg/kg neutralizing anti-BMP-7 antibody was injected every 3 days from day 2 to day 11. As a negative control, isotype-matched IgG2B (BD Biosciences) was injected at the same time points. Neutralizing activity of the antibody was evaluated by an assay measuring the production of alkaline phosphatase activity by C2C12 cells, as previously described (21).

In situ hybridization. The kidneys were excised from adult male mice and fixed in 4% paraformaldehyde in PBS. Frozen sections (5 μm thick) were treated with 1 μg/ml proteinase K in PBS at 37°C for 30 minutes and acetylated in 0.1 M triethanolamine-HCl, 0.25% acetic anhydride for 15 minutes. Hybridization was performed with probes at concentrations of about 1 μg/ml in a hybridization solution (50% formamide, ×5 SSC, 1% SDS, 50 μg/ml transfer RNA, and 50 μg/ml heparin) at 60°C for 16 hours. RNA probes were synthesized by in vitro transcription with a DIG RNA Labeling Mix (Roche Diagnostics Corp.). Each probe was designed to contain an open reading frame with the following length and G+C content: USAG-1, 1.0 kbp (G+C 52.6%); sclerostin, 1.5 kbp (61.7%); coco, 1.2 kbp (54.7%); DAN, 1.0 kbp (60.6%); twisted gastrulation, 0.7 kbp (55.1%); PRDC, 0.8 kbp (57.7%); chordin, 1.5 kbp (60.2%); gremlin, 0.9 kbp (50%); noggin, 0.7 kbp (64.7%); cerberus, 1.5 kbp (48.8%). Hybridization was detected using an anti-DIG AP conjugate (Roche Diagnostic Corp.) and NBT/BCIP solution (Roche Diagnostics Corp.).

Analysis of phenotype of adult teeth. Skeletal preparations of the maxillae and mandibles were made by soaking the mouse heads in 0.02% proteinase K in PBS at 37°C for 4 days after peeling off the skin, dissecting the maxillae and mandibles, and clearing them in 5% H_2O_2 at room temperature for 5 minutes. Finally they were rinsed in H_2O and left to dry.

Statistics. All assays were performed in triplicate. Data are presented as mean ± SD. Statistical significance was assessed by ANOVA, followed by Fisher's protected least significant difference post-hoc test. Survival curves were derived using the Kaplan-Meier method and compared using log-rank test.

Acknowledgments

We are grateful to Y. Nabeshima, T. Nakahata, and T. Nakamura for helpful discussion. We are grateful to M. Yoshimoto for hematological evaluation of the mice. We thank A. Godo, H. Uchiyama, and A. Hosoya for technical assistance. We thank W. Gray for reading the manuscript.

Received for publication April 25, 2005, and accepted in revised form October 11, 2005.

Address correspondence to: Motoko Yanagita, COE Formation for Genomic Analysis of Disease Model Animals with Multiple Genetic Alterations, Graduate School of Medicine, Kyoto University, Shogoin Kawahara-cho 54, Kyoto 606-8507, Japan. Phone: 81-75-751-3465; Fax: 81-75-751-3574; E-mail: motoy@kuhp.kyoto-u.ac.jp.

1. Eddy, A.A. 1996. Molecular insights into renal interstitial fibrosis. *J. Am. Soc. Nephrol.* **7**:2495–2508.
2. van Kooten, C., Daha, M.R., and van Es, L.A. 1999. Tubular epithelial cells: a critical cell type in the regulation of renal inflammatory processes. *Exp. Nephrol.* **7**:429–437.
3. Neilson, E.G. 2005. Setting a trap for tissue fibrosis. *Nat. Med.* **11**:373–374.
4. Zeisberg, M., et al. 2003. BMP-7 counteracts TGF-beta1-induced epithelial-to-mesenchymal transition and reverses chronic renal injury. *Nat. Med.* **9**:964–968.
5. Vukicevic, S., et al. 1998. Osteogenic protein-1 (bone morphogenetic protein-7) reduces severity of injury after ischemic acute renal failure in rat. *J. Clin. Invest.* **102**:202–214.
6. Hruska, K.A., et al. 2000. Osteogenic protein-1 prevents renal fibrogenesis associated with ureteral obstruction. *Am. J. Physiol. Renal. Physiol.* **279**:F130–F143.
7. Hruska, K.A. 2002. Treatment of chronic tubulointerstitial disease: a new concept. *Kidney Int.* **61**:1911–1922.
8. Zeisberg, M., et al. 2003. Bone morphogenic protein-7 inhibits progression of chronic renal fibrosis associated with two genetic mouse models. *Am. J. Physiol. Renal. Physiol.* **285**:F1060–F1067.

9. Dudley, A.T., Lyons, K.M., and Robertson, E.J. 1995. A requirement for bone morphogenetic protein-7 during development of the mammalian kidney and eye. *Genes Dev.* **9**:2795–2807.
10. Luo, G., et al. 1995. BMP-7 is an inducer of nephrogenesis, and is also required for eye development and skeletal patterning. *Genes Dev.* **9**:2808–2820.
11. Ozkaynak, E., et al. 1990. OP-1 cDNA encodes an osteogenic protein in the TGF-beta family. *EMBO J.* **9**:2085–2093.
12. Gould, S.E., Day, M., Jones, S.S., and Dorai, H. 2002. BMP-7 regulates chemokine, cytokine, and hemodynamic gene expression in proximal tubule cells. *Kidney Int.* **61**:51–60.
13. Simon, M., et al. 1999. Expression of bone morphogenetic protein-7 mRNA in normal and ischemic adult rat kidney. *Am. J. Physiol.* **276**:F382–F389.
14. Wang, S.N., Lapage, J., and Hirschberg, R. 2001. Loss of tubular bone morphogenetic protein-7 in diabetic nephropathy. *J. Am. Soc. Nephrol.* **12**:2392–2399.
15. Lund, R.J., Davies, M.R., and Hruska, K.A. 2002. Bone morphogenetic protein-7: an anti-fibrotic morphogenetic protein with therapeutic importance in renal disease. *Curr. Opin. Nephrol. Hypertens.* **11**:31–36.
16. Almanzar, M.M., et al. 1998. Osteogenic protein-1 mRNA expression is selectively modulated after acute ischemic renal injury. *J. Am. Soc. Nephrol.* **9**:1456–1463.
17. Massague, J., and Chen, Y.G. 2000. Controlling TGF-beta signaling. *Genes Dev.* **14**:627–644.
18. Simmons, D.G., and Kennedy, T.G. 2002. Uterine sensitization-associated gene-1: a novel gene induced within the rat endometrium at the time of uterine receptivity/sensitization for the decidual cell reaction. *Biol. Reprod.* **67**:1638–1645.
19. Avsian-Kretchmer, O., and Hsueh, A.J. 2004. Comparative genomic analysis of the eight-membered ring cystine knot-containing bone morphogenetic protein antagonists. *Mol. Endocrinol.* **18**:1–12.
20. Laurikkala, J., Kassai, Y., Pakkasjarvi, L., Thesleff, I., and Itoh, N. 2003. Identification of a secreted BMP antagonist, ectodin, integrating BMP, FGF, and SHH signals from the tooth enamel knot. *Dev. Biol.* **264**:91–105.
21. Yanagita, M., et al. 2004. USAG1: a bone morphogenetic protein antagonist abundantly expressed in the kidney. *Biochem. Biophys. Res. Commun.* **316**:490–500.
22. Schrier, R.W. 2002. Cancer therapy and renal injury. *J. Clin. Invest.* **110**:743–745. doi:10.1172/JCI200216568.
23. Megyesi, J., Safirstein, R.L., and Price, P.M. 1998. Induction of p21WAF1/CIP1/SDI1 in kidney tubule cells affects the course of cisplatin-induced acute renal failure. *J. Clin. Invest.* **101**:777–782.
24. Ramesh, G., and Reeves, W.B. 2002. TNF-α mediates chemokine and cytokine expression and renal injury in cisplatin nephrotoxicity. *J. Clin. Invest.* **110**:835–842. doi:10.1172/JCI200215606.
25. Yang, J., and Liu, Y. 2001. Dissection of key events in tubular epithelial to myofibroblast transition and its implications in renal interstitial fibrosis. *Am. J. Pathol.* **159**:1465–1475.
26. Klahr, S., and Morrissey, J. 2002. Obstructive nephropathy and renal fibrosis. *Am. J. Physiol. Renal. Physiol.* **283**:F861–F875.
27. Chevalier, R.L. 1999. Molecular and cellular pathophysiology of obstructive nephropathy. *Pediatr. Nephrol.* **13**:612–619.
28. Sato, M., Muragaki, Y., Saika, S., Roberts, A.B., and Ooshima, A. 2003. Targeted disruption of TGF-beta1/Smad3 signaling protects against renal tubulointerstitial fibrosis induced by unilateral ureteral obstruction. *J. Clin. Invest.* **112**:1486–1494. doi:10.1172/JCI200319270.
29. Kalluri, R., and Neilson, E.G. 2003. Epithelial-mesenchymal transition and its implications for fibrosis. *J. Clin. Invest.* **112**:1776–1784. doi:10.1172/JCI200320530.
30. Bottinger, E.P., and Bitzer, M. 2002. TGF-beta signaling in renal disease. *J. Am. Soc. Nephrol.* **13**:2600–2610.
31. Iwano, M., et al. 2002. Evidence that fibroblasts derive from epithelium during tissue fibrosis. *J. Clin. Invest.* **110**:341–350. doi:10.1172/JCI200215518.
32. Zeisberg, M., Shah, A.A., and Kalluri, R. 2005. Bone morphogenic protein-7 induces mesenchymal to epithelial transition in adult renal fibroblasts and facilitates regeneration of injured kidney. *J. Biol. Chem.* **280**:8094–8100.
33. Gerritsma, J.S., van Kooten, C., Gerritsen, A.F., van Es, L.A., and Daha, M.R. 1998. Transforming growth factor-beta 1 regulates chemokine and complement production by human proximal tubular epithelial cells. *Kidney Int.* **53**:609–616.
34. Li, T., Surendran, K., Zawaideh, M.A., Mathew, S., and Hruska, K.A. 2004. Bone morphogenetic protein 7: a novel treatment for chronic renal and bone disease. *Curr. Opin. Nephrol. Hypertens.* **13**:417–422.
35. Davies, M.R., Lund, R.J., Mathew, S., and Hruska, K.A. 2005. Low turnover osteodystrophy and vascular calcification are amenable to skeletal anabolism in an animal model of chronic kidney disease and the metabolic syndrome. *J. Am. Soc. Nephrol.* **16**:917–928.
36. Gonzalez, E.A., et al. 2002. Treatment of a murine model of high-turnover renal osteodystrophy by exogenous BMP-7. *Kidney Int.* **61**:1322–1331.
37. Hruska, K.A., et al. 2004. Kidney-bone, bone-kidney, and cell-cell communications in renal osteodystrophy. *Semin. Nephrol.* **24**:25–38.
38. Lund, R.J., Davies, M.R., Brown, A.J., and Hruska, K.A. 2004. Successful treatment of an adynamic bone disorder with bone morphogenetic protein-7 in a renal ablation model. *J. Am. Soc. Nephrol.* **15**:359–369.
39. Simic, P., and Vukicevic, S. 2005. Bone morphogenetic proteins in development and homeostasis of kidney. *Cytokine Growth Factor Rev.* **16**:299–308.
40. Davies, M.R., Lund, R.J., and Hruska, K.A. 2003. BMP-7 is an efficacious treatment of vascular calcification in a murine model of atherosclerosis and chronic renal failure. *J. Am. Soc. Nephrol.* **14**:1559–1567.
41. Hruska, K.A., Mathew, S., and Saab, G. 2005. Bone morphogenetic proteins in vascular calcification. *Circ. Res.* **97**:105–114.
42. Godin, R.E., Takaesu, N.T., Robertson, E.J., and Dudley, A.T. 1998. Regulation of BMP7 expression during kidney development. *Development.* **125**:3473–3482.
43. Michos, O., et al. 2004. Gremlin-mediated BMP antagonism induces the epithelial-mesenchymal feedback signaling controlling metanephric kidney and limb organogenesis. *Development.* **131**:3401–3410.
44. Itasaki, N., et al. 2003. Wise, a context-dependent activator and inhibitor of Wnt signalling. *Development.* **130**:4295–4305.
45. Lin, J., et al. 2005. Kielin/chordin-like protein, a novel enhancer of BMP signaling, attenuates renal fibrotic disease. *Nat. Med.* **11**:387–393.
46. Nishida, M., et al. 2002. Absence of angiotensin II type 1 receptor in bone marrow-derived cells is detrimental in the evolution of renal fibrosis. *J. Clin. Invest.* **110**:1859–1868. doi:10.1172/JCI200215045.
47. Yanagita, M., et al. 2001. Gas6 regulates mesangial cell proliferation through Axl in experimental glomerulonephritis. *Am. J. Pathol.* **158**:1423–1432.
48. Yanagita, M., et al. 2001. Gas6 induces mesangial cell proliferation via latent transcription factor STAT3. *J. Biol. Chem.* **276**:42364–42369.
49. Yanagita, M., et al. 2002. Essential role of Gas6 for glomerular injury in nephrotoxic nephritis. *J. Clin. Invest.* **110**:239–246. doi:10.1172/JCI200214861.